6-2019

Thermal Characterization of Graphene/Polyethylene Nanocomposites

Ahmed Z. A. Abuibaid

Recommended Citation

A. Abuibaid, Ahmed Z., "Thermal Characterization of Graphene/Polyethylene Nanocomposites" (2019). *Chemical and Petroleum Engineering Theses*. 4.
https://scholarworks.uaeu.ac.ae/chem_petro_theses/4

جامعة الإمارات العربية المتحدة
United Arab Emirates University

United Arab Emirates University

College of Engineering

Department of Chemical and Petroleum Engineering

THERMAL CHARACTERIZATION OF GRAPHENE/POLYETHYLENE NANOCOMPOSITES

Ahmed Z. A. Abuibaid

This thesis is submitted in partial fulfilment of the requirements for the degree of Master of Science in Chemical Engineering

Under the Supervision of Dr. Muhammad Iqbal

June 2019

Declaration of Original Work

I, Ahmed Z. A. Abuibaid, the undersigned, a graduate student at the United Arab Emirates University (UAEU), and the author of this thesis entitled "*Thermal Characterization of Graphene/Polyethylene Nanocomposites*", hereby, solemnly declare that this thesis is my own original research work that has been done and prepared by me under the supervision of Dr. Muhammad Iqbal, in the College of Engineering at UAEU. This work has not previously been presented or published, or formed the basis for the award of any academic degree, diploma or a similar title at this or any other university. Any materials borrowed from other sources and relied upon or included in my thesis have been properly cited and acknowledged in accordance with appropriate academic conventions. I further declare that there is no potential conflict of interest with respect to the research, data collection, authorship, presentation and/or publication of this thesis.

Student's Signature: Ahmad Date: 4/7/2018

Approval of the Master Thesis

This Master Thesis is approved by the following Examining Committee Members:

1) Advisor (Committee Chair): Dr. Muhammad Zafar Iqbal
   Title: Assistant Professor
   Department of Chemical and Petroleum Engineering
   College of Engineering

   Signature ______________ Date 06/27/2019

2) Member (Internal Examiner): Professor Nayef Ghasem
   Title: Professor
   Department of Chemical and Petroleum Engineering
   College of Engineering

   Signature ______________ Date 27/6/2019

3) Member (External Examiner): Professor Andrew M. Herring
   Title: Professor
   Department of Chemical and Biological Engineering
   Institution: Colorado School of Mines, USA

   Signature ______________ Date 30/6/2019

This Master Thesis is accepted by:

Dean of the College of Engineering: Professor Sabah Alkass

Signature Sabah Date 4/7/2019

Acting Dean of the College of Graduate Studies: Professor Ali Al Marzouqi

Signature Ali Hassan Date 4/7/2019

Copy ____ of ____

Abstract

Practically, almost all polymers are solidified from the melts for product-forming purposes. Therefore, the evolution of solid structure (crystallization behavior) from their molten form has prime importance in manufacturing high performance materials.

Polyethylene (PE) is one of the most commonly used semicrystalline polymers all over the world. In this thesis, nanocomposites of PE with thermal reduced graphene (TRG) (PE/TRG) were prepared via solvent blending and the crystallization of PE has been investigated using a differential scanning calorimeter (DSC). The nanocomposites were crystallized from the melts under both isothermal and dynamic conditions, and evolution of crystal formation is studied using kinetic analysis. The kinetic data obtained from isothermal crystallization experiments showed excellent fit with the Avrami kinetic theory whereas the dynamic data was better described via Ozawa kinetic model. The parametrization of crystallization process was carried out using various models in order to understand energetics involved during crystallization (solidification) of PE/TRG nanocomposites. The Hoffman-Lauritzen energetic theory further confirmed that inclusion of graphene reduced work required for crystallization, thus facilitating the kinetic growth of the crystals. The graphene nanosheets acted as nucleating agents by substantially decreasing the time to reach 50% of crystallization. The quantitative results from the kinetic analysis were consistent with other nanocomposites where the nanofillers acted as nucleating agents.

Keywords*:* Polyethylene, Graphene, Nanocomposites, Crystallization, DSC.

Title and Abstract (in Arabic)

الوصف الحراري لمركبات نانوكومبوسيت الجرافين / البولي إيثيلين

الملخص

عمليا، يتم تقوية جميع البوليمرات تقريبًا عن طريق الانصهار لأغراض تكوين المنتج. لذلك، فإن تطور الهيكل الصلب (سلوك التبلور) من شكله المنصهر له أهمية قصوى في تصنيع المواد عالية الأداء.

البولي ايثيلين (PE) هو واحد من البوليمرات شبه البلورية الأكثر استخداما في جميع أنحاء العالم. في هذه الرسالة، تم تحضير المركبات النانوية للـ PE مع الجرافين المخفض حراريًا (TRG) (PE/TRG) عبر مزج المذيبات وتم فحص تبلور الـ PE باستخدام مقياس المسعر التفاضلي للمسح (DSC). تم تبلور المركبات النانوية من الذوبان تحت كل من الظروف الحرارية والديناميكية، ويتم دراسة تطور تكوين البلورة باستخدام التحليل الحركي. أظهرت البيانات الحركية التي تم الحصول عليها من تجارب التبلور متساوي الحرارة توافقًا ممتازًا مع نظرية Avrami الحركية، في حين تم وصف البيانات الديناميكية بشكل أفضل عبر نموذج Ozawa الحركي. تم تنفيذ عملية تحديد معالم عملية التبلور باستخدام نماذج مختلفة لفهم علم الطاقة المتورط أثناء التبلور (التصلب) للمركبات النانوية PE /TRG. أكدت نظرية حيوية Hoffman-Lauritzen أن تضمين الجرافين يقلل من العمل اللازم لبلورة، وبالتالي تسهيل النمو الحركي للبلورات. كانت صفائح الجرافين النانوية بمثابة عوامل نواة عن طريق تقليل الوقت اللازم للوصول إلى 50% من التبلور. كانت النتائج الكمية من التحليل الحركي متسقة مع المركبات النانوية الأخرى حيث كان عامل النانو يعمل كعوامل النواة.

مفاهيم البحث الرئيسية: بولي ايثيلين، الجرافين، النانوية، بلورة، المسح التفاضلي المسعر.

Acknowledgements

I would like to thank God for giving me the strength to complete this work. My first thanks go to my main supervisor Dr. Muhammad Zafar Iqbal, Department of Chemical and Petroleum Engineering, who guided me through the two years of research. I would like to thank them for providing me with the precious academic time to pursue my research goals.

In addition, I would like to thank Dr. Hussein Awad and Efstratios Svinterikos for their assistance with Raman, XRD and SEM characterizations.

Special thanks go to my parents, brothers, and sisters who helped me along the way. I am sure they suspected it was endless. In addition, special thanks are extended to Chemical and Petroleum Engineering doctors, staffs, and student for their assistance and friendship.

This work was financially supported by the UAE University Research Startup Grant (# 31N269).

Dedication

To my beloved parents and family

Table of Contents

List of Tables

List of Figures

List of Abbreviations

CB	Carbon Black
DSC	Differential Scanning Colorimeter
FWHM	Full Width at Half Maximum
GO	Graphite Oxide
ΔH_c	Crystallization Enthalpy
ΔH_m	Melting Enthalpy
LLDPE	Linear Low-Density Polyethylene
PE	Polyethylene
PET	Polyethylene terephthalate
PVA	Vinyl Alcohol
SEM	Scanning Electron Microscopy
T_c	Crystallization Temperature
TEM	Transmission Electron Microscope
T_g	Glass Transition Temperature
T_m	Melting Temperature
TRG	Thermal Reduced Graphene
UV	Ultra-Violet
X_c	Percentage of Crystallinity
XRD	X-ray Diffractometer

Chapter 1: Background

1.1 Overview

With fast developing nanotechnology, polymeric materials are quickly replacing the conventional materials for many applications due to the characteristics such as good elongation, lightweight, toughness, easy processing, and low cost [1]. On the other hand, polymers comparing to metals show a high gas permeability, low strength, stiffness and flammability as shortcomings. That is why inorganic materials (fillers) are sometimes required to reinforce polymers to meet property expectations.

1.2 Amorphous vs crystalline polymers

When the polymer melt solidifies in a glassy-like behavior, the molecular chains are characterized by the absence of long-range order [2]. A polymer lacking the long-range order is also called an amorphous polymer. The amorphous state can be specified by the absence of first-order melting transition and any X-ray diffraction patterns.

Amorphous polymers form only a weak short-range structure ranging from ~10 nm - 50 nm [2]. Figure 1 shows different structural forms for the amorphous state. The models in this figure are sorted from low to high degree order. The development of random coil by Flory led to a description of the confirmation of chains[3]. Privalko and Lipatov developed the relation between folded-chain model and random coil[4]. The Folded-chain fringed-micellar grain model [5] consists of two elements: the inter-grain region of randomly packed chains, and grain (ordered) domain of quasi-parallel chains. Pechhold made the highest order model between others. In this model, the defective bundle structure with meander-like folds [6].

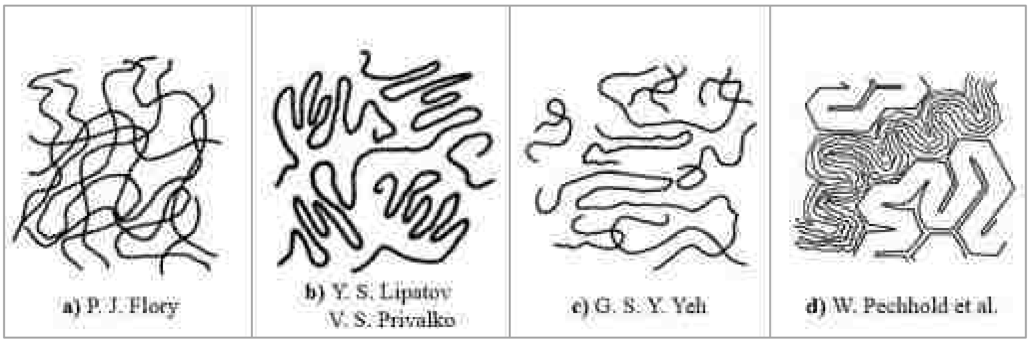

Figure 1: Amorphous state models. (a) The random coil; (b) The randomly folded chain conformations; (c) Folded-chain fringed- micellar; and (d) Meander model.

On the other hand, the crystalline polymers generally exhibit high rigidity, strength and ordered chain structure. When polymers are crystallized in the bulk state, the individual crystallites are microscopic or even submicroscopic in size. They are an integral part of the solids and cannot be isolated. Hence, studies on crystalline polymers in the bulk were limited to powder diagrams of the Debye-Scherrer type or fiber diagrams of oriented materials [7, 8]. In Figure 2, a single crystal of polyethylene was investigated using electron microscopy and electron diffraction. The structural of the single-crystal polyethylene is typically diamond-shaped.

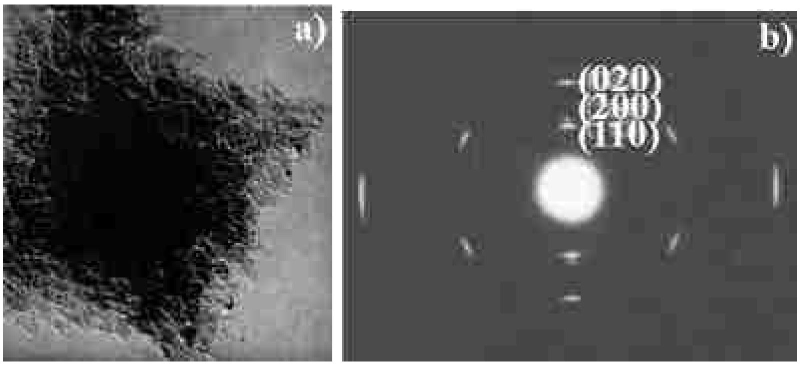

Figure 2: Polyethylene single-crystal structure under a) electron microscopy. b) Electron diffraction with identical orientation. (reproduced with permission from [9, 10]).

1.3 Semicrystalline polymer

Since there is no perfectly amorphous or crystalline polymer, all polymers are considered semicrystalline. Semicrystalline polymers exhibit the behavior of amorphous and crystalline phases. In general, the semicrystalline polymers show a higher degree of complexity in dynamic-mechanical properties than that of the amorphous ones resulting in changes in the orientation and the order of segments in polymer molecules. In addition, eventually, semicrystalline polymers exhibit a different degree of crystallinity and crystalline forms, subsequently leading effect morphology, structure, and properties of the polymers [11, 12].

The addition of nanofiller to the semicrystalline polymers would alter the arrangement of packing of the polymer chain, resulting in the formation of lamellar and spherulite structures. Figure 3 illustrates the shish-kebab structure of pure polymer after the addition of the nanotube. The nanotube eliminates or reduces the very high-stress fields that accompany with elongated pure polymer chains [13].

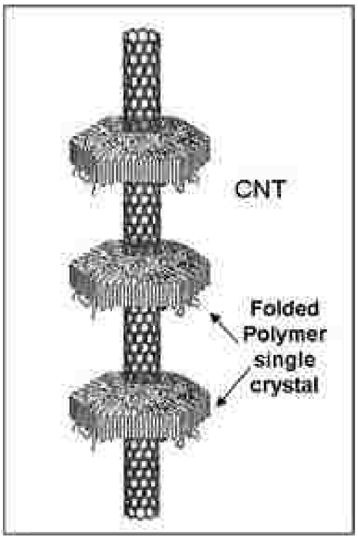

Figure 3: Schematic of the shish-kebab structure of pure polymer with nanotube filler (reproduced with permission from [13]).

1.4 Polymer nanocomposites

Polymers industry started to expand in the 19th century when inorganic particles (called fillers) were added into polymers to improve their properties (polymer composites) [14]. Fillers are classified into two groups: reinforcing fillers and non-reinforcing fillers. The reinforcing fillers improve functional properties of polymers with the addition of the fillers such as metallic powders, graphite, silica, and carbon black. On the other hand, nonreinforcing fillers such as calcium carbonate, and wheat flour, etc. are added to alter the color, reduce the price or change transparency [7]. However, with the advent of nanofillers such as nanosilica, the mechanism of improving functional properties of polymers changed.

Nanotechnology refers broadly to the understanding and control of matter at the dimensions of 1 to 100 nanometers [14]. Nanotechnology is playing a major role in science and engineering fields. The nanomaterials have introduced intriguing discoveries in areas such as measuring, imaging, manipulating, and modeling matter at nano-length scale. In various applications, nanotechnology and nanomaterial are also used for cost-effective technologies [15, 16].

Polymer nanocomposites have shown enormous potential in various applications since 1960. A mixture of nanotechnology and polymer science revealed the development of materials with outstanding mechanical, unique chemical and physical properties due to the high surface area to volume ratio of nanomaterials. Similarly, electrically and thermally conductive polymer nanocomposites have introduced important applications in the areas such as adhesives, sensors, antistatic coatings and films, actuators, and electromagnetic interference shielding materials for electronic devices [1, 14-22].

1.5 Graphene/polymer nanocomposites

Graphene, a two dimensional, 1-atom thick layer of sp^2-hybridized carbons arrange in a honeycomb-like network. It has proved to be a versatile filler for polymer nanocomposites. It has the ability to change its shape as rolled into one-dimensional nanotube and stacked into three-dimensional graphite or into zero-dimensional fullerenes (more examples are shown in Figure 4). It is an ideal material for electrical conductivity due to Near-ballistic transport and high mobility. Other properties such as mechanical and optical properties find its place in the micro- and nanomechanical systems [23-28].

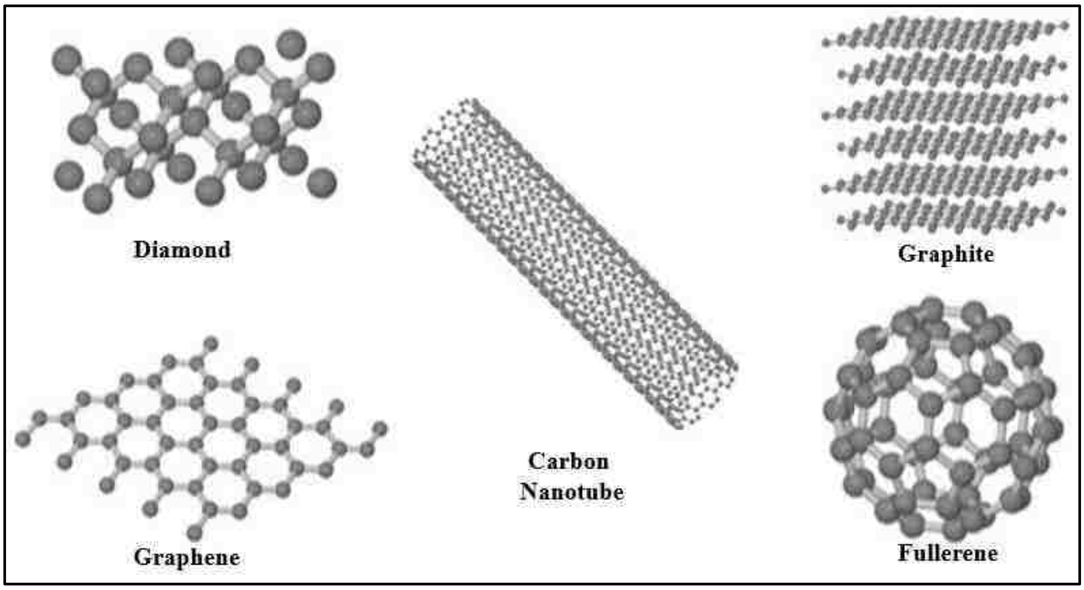

Figure 4: Allotropic forms of graphite

There are many procedures to produce graphene. A method that is simple and effective is by rubbing layered crystal with another marital surface. It forms flakes attached to the marital surface always in a single layer [29]. Another method of producing the graphene is by fabrication (Figure 5). A study was done by Zhang on 2004[30], which used a highly oriented pyrolytic graphite to extract graphene. In this study, graphite was fabricated by micropatterning on a highly oriented pyrolytic graphite surface. After that, a pillar from graphite was removed from the surface and glued down by a small amount of ultraviolet sensitive epoxy. Then the graphite sample was cleaved into SiO_2/Si surface using AFM (Nanoscope IIIa Multimode, Digital Instruments). Finally, the cleaved graphite samples were fabricated by electron beam lithography.

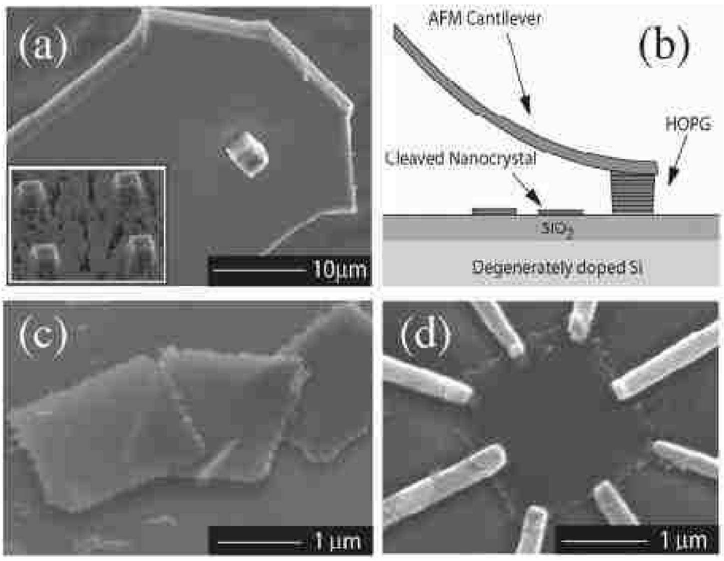

Figure 5: Producing the graphene is by fabrication (a)SEM of highly oriented pyrolytic graphite. (b) Schematic drawing of the micro-cleaving process. (c) a cleaved graphite samples. (d) fabrication of leaved graphite samples. (reproduced with permission from [30]).

The most important step in the preparation of the nanocomposites is to maximize dispersion of the nanofillers in the polymer matrix. The maximum reinforcement in a nanocomposite can be achieved if filler particles are well dispersed in the polymer leading to filler/polymer molecular-level interactions. A procedure was proposed by Bunnell [31] for the production of nanocomposites. In this work, polymer nanocomposite was incorporated with graphite nanoplatelets exfoliated from thermal treatment or shear grinding. Furthermore, Macosko and Kim [30] investigate the effect of the blending methods on the properties of the sample. They conclude that the dispersion is shown a better yield in solvent blending than melt compounding. The electrical conductivity of the polyethylene/Thermal reduced graphene TRG/ enhancement had improved more than reduced graphene in functionalized polyethylene. The graphene/polymer nanocomposites can be made through various methods such as in-situ polymerization, solvent blending and melt blending.

The *in-situ* polymerization involves polymerization of a monomer in the presence of filler. The fillers are usually covalently bonded with the monomers molecules which grow into polymer chains leading to improved dispersion in nanocomposites [15]. The nanocomposite produced by this method is usually thermally stable and insoluble polymer [32]. One of the main drawbacks of this method is exponentially increased the viscosity of the mixture during the polymerization step, which requires too much energy of mixing in order to keep the mixture perfectly dispersed.

Mecking [33] performed *in-situ* polymerization of ethylene to prepare to polyethylene/graphene nanocomposites shown in Figure 6 and compared the results with melt mixed nanocomposites. The nanocomposites synthesized *in-situ* showed a significantly lower percolation threshold (2 wt% of graphene) compared to that of 20 wt% in melt processed nanocomposites.

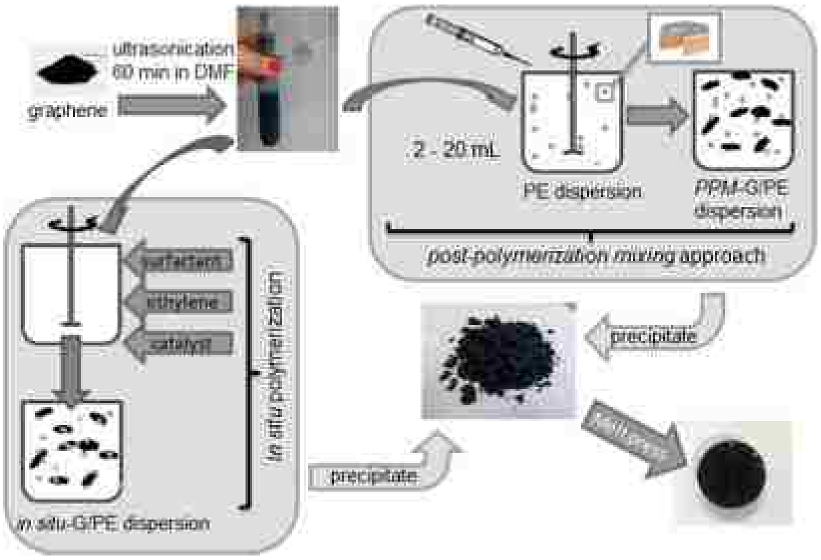

Figure 6: Preparation of PE/graphene composites by in situ polymerization, post-polymerization mixing, and precipitation methods. (reproduced with permission from [33]).

In the solution blending method, matrix polymer and fillers are dispersed in a suitable solvent. The solution blending method is well known for making small samples with maximum dispersion. The solution method is assumed to give a maximum dispersion of fillers in a polymer. However, the use of hazardous chemicals as the solvent is the main drawback in this method limiting its scale-up and commercialization [15, 33]. In this thesis, solution blending was used to prepare graphene/polymer nanocomposites. In general, solution blending consists of three main steps (Figure 7): 1) dispersing graphene in a suitable solvent, for example, p-xylene, 2) adding polyethylene into the solution and heating, and 3) finally, precipitating the nanocomposite mixture using a non-solvent or drop casting the solution to make dried nanocomposites.

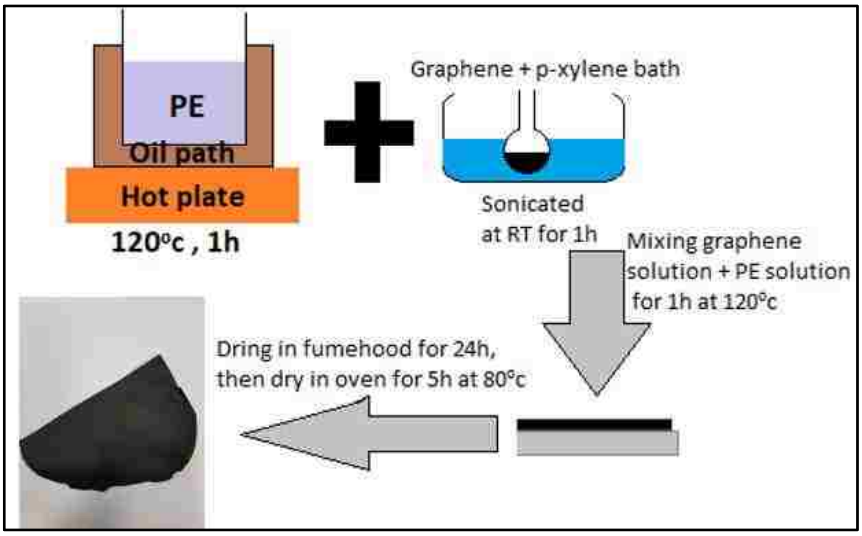

Figure 7: A typical example of the solution processing of graphene/polyethylene nanocomposites via drop cast method.

The most commonly used industrial method of mixing fillers in polymers is via melt blending approach. Typically, heating polymer pellets in a solvent to make a viscous solution followed by dispersing nanomaterial requires high shear force and frequent disposal of hazardous solvents. On the other hand, the melt blending approach does not involve any solvent, regarded as the cheapest and easiest method for manufacturing polymer nanocomposites. This is the most preferred method at an industrial scale since it provides large production at a lower cost [15, 34]. Regarding the dispersion of fillers in polymer, the melt blending approach offers the poorest dispersion practically.

Due to poor dispersion in melt blending, Song [35] combined *in-situ* and melt blending methods to manufacture high-density polyethylene/graphene nanocomposites. The nanocomposite was prepared initially by *in-situ* polymerization and subsequently, the nanocomposites were melt blended in a twin-screw extruder (Figure 8). The resultant nanocomposites showed a marked increase in mechanical properties of the nanocomposites compared with those prepared by any of the above method individually, attributed to improved dispersion of graphene in polyethylene.

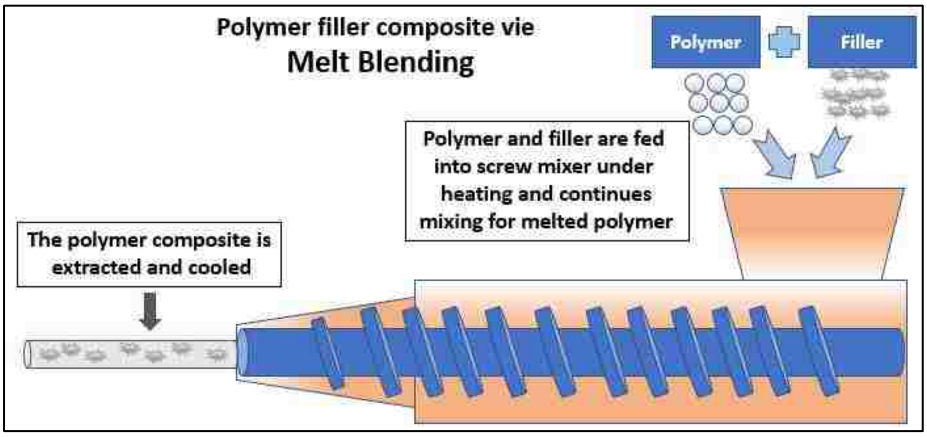

Figure 8: A simplified representation of the melt blending technique

1.6 Polymer crystallization

Whether the polymer is thermoset or thermoplastic, the heating/cooling processes are necessary for the production of products. Typically, thermoplastics product formation requires producing molten polymers via heating followed by solidification via cooling.

Since both heating and cooling cycles are essential for product formation, cooling the molten polymer from the melt produces various levels of properties depend on the cooling rate for a typical polymer to solidify. The polymer chains rearrange themselves upon the solidification leading to unique properties. Polymer extrusion, injection molding, thermoforming, and rotational molding are some examples of polymer processing techniques in which heating/cooling cycles are essential [36].

As mentioned earlier, incorporation of a filler to make nanocomposites alters mechanical, electrical, and thermal properties (functional properties) of the nanocomposites. In addition to that, fillers also affect the crystallization/solidification behavior of the polymer. Therefore, polymer crystallization in the presence of filler/nanofillers is an essential process in polymer science and it holds the key to understanding final polymer behavior. Broadly, polymer solidification/crystallization studies are involved in understanding morphology of polymer nanocomposites, the formation of a crystalline compound, and entrapping nanoparticles in polymer blends, and optical properties and mechanical properties of the final product [37].

In crystallization, bond orientation, long-range positions, and molecular orientational orders with respect to the arrangement of the structural unit of the polymers (motif) are the important characteristics of a crystal. The motif is defined as the smallest repeating structural unit that is a form of atoms, ions, parts of a molecule, a whole molecule, or even a group of molecules [38].

A crystal begins to form from a tiny crystal called nucleus. The nucleus is the initiation of the crystallization in polymers. The formation of crystals is connected with two opposite thermodynamic energies: 1) a stabilizing negative bulk Gibbs free energy, and 2) a destabilizing positive free surfaces energy [37]. For the nucleus, the free surfaces energy has a higher value than bulks Gibbs free energy. For that reason, the overall free energy is positive and called a nucleation barrier. The general equation for calculating the nucleation barrier can be expressed as:

$$\Delta G = -V\,\Delta g_f + A_{\gamma} + B_{\gamma_e}$$

Here, A and B are the lateral and fold-surface areas, γ and γ_e are densities of the lateral and fold-surface free energy respectively, and Δg_f is the bulk Gibbs free energy change with a crystal volume of V. The ΔG is the driving force for the crystallization process (Gibbs free energy) which is the difference between the initial (isotropic liquid) and the final (crystal) states [37, 39].

Initially, in 1903, the crystal growth in polymers was proposed to be defined as the surface nucleation process that occurs after the first nucleation step (primary nucleation) [37]. This primary nucleation occurs at a lower crystallization temperature comparing to the surface nucleation that takes a higher crystallization temperature. Thereafter, after primary nucleation, the crystal growth is identified as a surface nucleation-controlled phenomenon. However, this case of kinetic development of crystals can only happen when the crystal growth is located on an atomically smooth surface. This step requires a nucleation barrier. The nucleation-controlled by the lowest crystal growth plane in which a formed sector of macroscopic facets results in single crystal growth is also called lateral growth.

The continuous growth model is another kinetics growth mechanism. In this model, impingement sites on an atomically rough surface become potential growth sites. The temperature and/or concentration are the reason for shaping the single crystal in this model. Usually, curved crystals are obtained as an indication of continuous growth mechanism [7, 37-39]. Figure 9 represents a typical representation of different crystal formation processes in a polymer.

In polymer science, crystallization is divided into two types: 1) isothermal crystallization where the crystals are grown at fixed temperatures, and 2) nonisothermal crystallization where dynamic cooling is applied to make instant crystals. In the following section, a brief detail of these processes is provided.

1.6.1 Isothermal crystallization

Typically, in the isothermal crystallization process, a polymer is melted above its melting point and subsequently cooled to a fixed temperature where crystals are expected to grow isothermally. The development/evolution of crystal growth can be tracked using various thermal analysis instruments. The most commonly used instruments are dilatometry, small angle and wide-angle X-ray scattering, and calorimeter. In addition, the isothermal technique attracts the researchers around the globe since it offers a vast theoretical understanding of crystal formation [40].

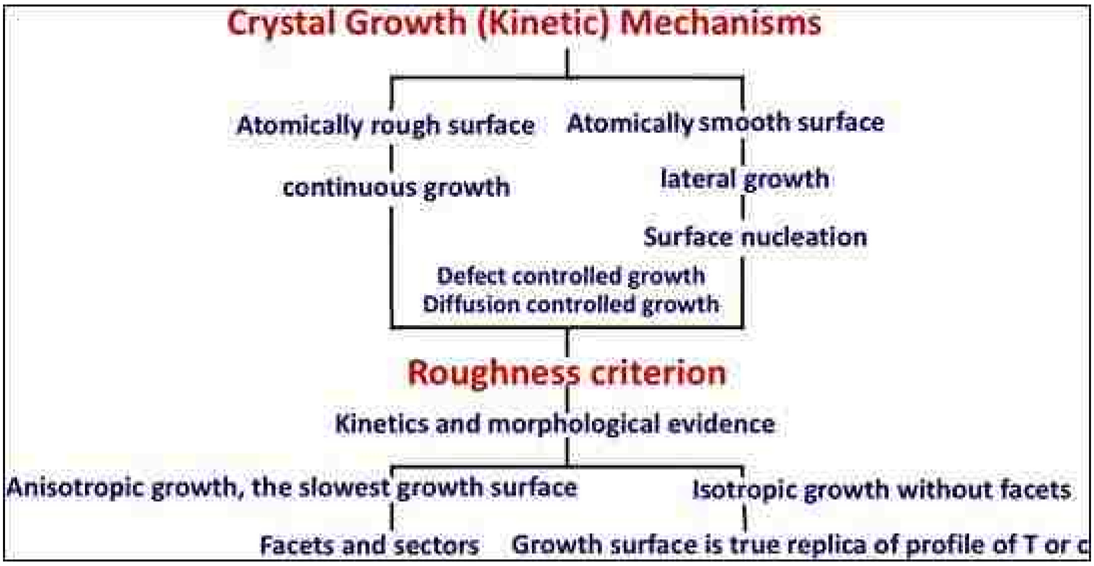

Figure 9: Summary of crystal growth mechanism

One of the most popular theories to track the isothermal kinetic data is the Avrami equation. The Avrami theory evaluates the linear growth of crystals with a constant nucleation rate. Numerous possibilities can be considered with a broad variety of expressions in the one-, two- or three-dimensions growth of crystals [41]. Typically, only two- and three-dimensions crystal morphologies are obtained as axialites and spherulites respectively. The theory further provides an index to identify the nucleation rate of polymers between completely sporadic or completely sporadic crystals [42].

The Hoffman and Lauritzen theory (HL) is another important theory to investigate the energetics of the kinetics of an isothermal process. The theory assumes that lamellar formation and chain folding are kinetically controlled, meaning the crystals are actually the metastable form developed during the solidification process [7]. A schematic is shown in Figure 10 depicting a basic model of crystal formation as hypothesized by the Hoffman and Lauritzen theory. Here in the Figure, x the large dimension, ℓ the is the thin dimension of the crystal, σ the lateral surface interfacial free energy, and σe the fold-surface interfacial free energy.

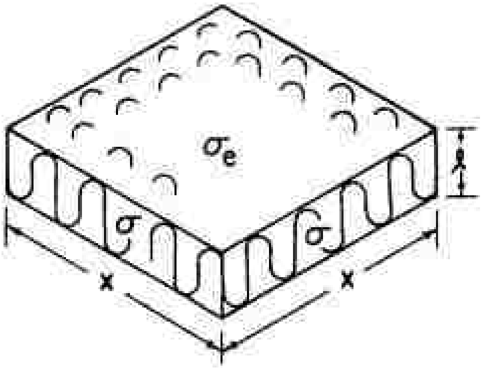

Figure 10: Represented crystal chain-folded by Hoffman and Lauritzen theory (reproduced with permission from ref [7])

1.6.2 Nonisothermal crystallization

The nonisothermal crystallization process has a great weight in the industrial sector as catches the real picture of crystallization in practical applications. This method requires a series of different cooling rate to obtain the kinetics and the optimal cooling rate to achieve the best properties of the polymer sample are evaluated.

Cooling the polymer from the melt is similar to passing through a succession of isotherms at each different crystallization temperature [40, 43].

The theory behinds the nonisothermal crystallization kinetics are the same as the isothermal method such as the Avrami theory, and Hoffman and Lauritzen theory. In addition to that, Ozawa theory can be applied to the nonisothermal process.

The Ozawa theory assumes the crystallization of a sample occurs at a constant crystal grow and a constant rate from an initial distribution of the nuclei in the form of spherulites (three-dimensional crystals with a constant growth radius at a given temperature) [44]. The Ozawa theory uses temperature-dependent relative crystallinity, X (T) as a function of the cooling rate (φ)), represented as follows [45]:

$$1 - X\left(T\right) = \exp\left(-k(T) / \varphi^{n}\right)$$

Here, k (T) is the crystallization rate constant (a function of temperature), and n = m + 2 where m is the Ozawa's parameter which is a function of dimensions of the crystal growth and nucleation mechanism.

1.7 Objectives of the study

1.7.1 The general objective

This study is focused on understanding the thermal crystallization kinetics of polyethylene/graphene nanocomposites. Polyethylene is one of the most commonly used commodity polymer in the world, and many forms of polyethylene composites are already in the market with applications ranging from plastic bags to coating wires. Therefore, it will be of high importance to understand how graphene can alter the crystallization behavior of polyethylene.

Specifically, the study deals with the following specific objectives:

1) Analysis of isothermal crystallization data for graphene/polyethylene nanocomposites and fitting the experimental data with kinetic theory.
2) Analysis of nonisothermal crystallization data for graphene/polyethylene nanocomposites and fitting the experimental data with kinetic theory.
3) Understanding the energetics of crystal formation as a function of Gibb's free energy and surface energy.
4) Comparing graphene/polyethylene nanocomposites with conventional carbon black/polyethylene composites prepared by the same method.

1.7.2 Approach

This study involves the following tasks:

1) Synthesis of thermally reduced graphene via simultaneous thermal exfoliation and reduction of graphite oxide.
2) Preparation of polyethylene/graphene nanocomposites and polyethylene/carbon black using solvent blending method.
3) Characterization of thermally reduced graphene.
4) Melt crystallization using Differential Scanning Calorimetry (isothermal and nonisothermal methods).
5) Analysis of kinetic data using various kinetic models.
6) Comparison with conventional carbon black/polyethylene composites.

Chapter 2: Melt Crystallization of Graphene/Polyethylene Nanocomposites

2.1 Introduction

Polymer nanocomposites containing nanofillers with high-performance properties have attracted both academia and industry during the last few decades. The nanocomposites have outperformed the conventional composite market in functional properties such as thermal and electrical conductivity, and mechanical and thermal properties at very low filler loadings [17-20]. Among various nanofillers, graphene has shown enormous potential in increasing the specific functional properties of the polymers compared to other nanofillers available in the market [25].

Semicrystalline polymers (e.g., PE, PVA, PET, and more) constitute an important class of polymers for nanocomposite applications. These polymers crystallize when cooled from the melt or heated from the amorphous state to the temperature regime between T_g and T_m. Due to the presence of significant amorphous fractions between the crystals, the crystallization can result in various forms such as single crystals, polycrystalline aggregates, and highly oriented structures. However, the overall kinetics of crystallization can be characterized by a degree of conversion and conversion rate, irrespective of the structures encountered. Practically, crystallized polymer properties strongly depend on the crystalline structure formed during processing [46]. For semicrystalline polymers such as PE and iPP which do not show cold crystallization, crystals can be formed isothermally (at selected temperatures) or nonisothermally (at variable cooling rates) while cooling from the melt. The isothermal crystallization is mostly used for theoretical analysis. However, practical processing methods such as extrusion, injection molding, and film blowing are performed under dynamic, nonisothermal conditions. Therefore, quantifying crystallization rates (isothermal and nonisothermal) is pertinent in optimizing industrial processes.

Generally, the surface/volume ratio increases with decreasing the particle size of the fillers. A 100-fold increase in surface area of the particles is expected with a 10-fold decrease in particle diameter (one of the main attractions towards the use of nanofillers). An interfacial polymer layer (shell) is attached to the particle (core) due to the large surface area of nanoparticles, forming an interface. The nanocomposites filled with less than 5 vol.% of the filler can be regarded as interfacial composites [46] where a large portion of the polymer is located at the polymer-particle interface. The molecular chain mobility is restricted in the shell compared to that in the bulk material, resulting in chain confinement effects in polymers, eventually increasing T_g. On the other hand, the reverse is true for noninteracting polymer-particle interfacial forces. Thus, in semicrystalline polymer nanocomposites, the polymer-nanoparticle adhesion is a function of the crystalline structure of polymer at the interface (shell), resulting in varied crystallinity, crystalline form, and morphology of the nanocomposites [46, 47]. These factors further result in altered physical properties of the nanocomposites (especially the mechanical properties). Consequently, in nanocomposites, understanding the effects of chemical and/or physical interactions on the crystalline structure as well as crystallization behavior is of great practical importance for product formation processes.

Graphene is a two-dimensional, one-atom-thick layer of sp^2-hybridized carbon atoms arranged in a honeycomb-like network. Thermally reduced graphene (TRG) is produced by simultaneous thermal exfoliation and reduction of graphite oxide [48] (a top-down method). High surface area TRG (1260 m^2/g) comprises of a few layers of 200 nm to a few microns wide graphene sheets with a thickness of 1-5 nm per TRG particle [49]. Typically, exceptionally high modulus of graphene (~1000 GPa in tension compared with ~1-10 GPa for polymers and 10-800 GPa for other fillers) makes it a versatile filler for polymer nanocomposites applications [50]. In graphene/polyethylene (PE) nanocomposites, Cheng et al. [51] reported crystallization of PE/reduced graphene oxide and showed accelerated crystallization of PE resulting in improved thermal stability of the nanocomposites compared to neat PE. A similar conclusion was reached by Fan et al. [52] using a compatibilizer in nanoclay/PE nanocomposites where nanoclay acted as a heterogeneous nucleating agent promoting the crystallization rate in the nanocomposites. Tarani et al. [43] reported fast crystallization of graphene/high-density polyethylene (HDPE) nanocomposites with variable graphene particle diameter. Higher cooling rates during nonisothermal crystallization process resulted in the formation of small-scale ordered-domains, lacking high-ordered structures in HDPE. In addition, bigger particles produced crystals with increased aggregate size. Recently, Iqbal et al. [53] reported PE/TRG nanocomposites and showed marked improvement in mechanical and electrical properties of nanocomposites via blending PE with oxidized PE. The increased properties were attributed to microstructural changes induced by TRG and oxidized PE into the PE structure. However, no crystallization data was reported to confirm the structural changes in PE with TRG.

This paper focuses on understanding how TRG affects the crystallization behavior of PE/TRG nanocomposites. The PE/TRG nanocomposites were crystallized isothermally and nonisothermally, and the kinetics of crystallization were studied. The evolution of crystal formation is systematically investigated with the help of the crystallization theories. Furthermore, the results from PE/TRG nanocomposites are also compared with conventional carbon black filled PE composites.

2.2 Experimental

2.2.1 Materials

Linear low-density polyethylene (LLDPE) with a bulk density 0.97 g/cm^3 (428078, lot#07730MEV, Sigma Aldrich), carbon black (CB) (99.9%, bulk density = 170-230 g/L, surface area = 75 m^2/g, Alfa Aesar), or Natural flake graphite (-10 mesh, 99.9% Alfa Aesar). p-xylene (99%, Sigma Aldrich), potassium permanganate (Fisher Scientific), sulfuric acid (95-97%, J.T. Bakers), phosphoric acid (>99%, Aldrich), hydrogen peroxide (30% solution, BDH), HCl (37%, Reidel-deHaen), were used as received.

2.2.2 Synthesis of Thermally Reduced Graphene (TRG)

TRG was prepared by simultaneous thermal exfoliation and reduction of graphite oxide (GO) [48, 53, 54]. The Tour's method was used to synthesize GO [54, 55]. Natural flake graphite (~5 g) was added into a mixture of sulfuric acid (272 mL) and phosphoric acid (33 mL) and kept under stirring for 30 min at room temperature. Potassium permanganate (~27.8 g) was slowly added to this mixture (in 3-5 minutes on average). The resulting mixture was stirred using an overhead stirrer for three days at room temperature. Upon completion of the reaction, 30% solution of hydrogen peroxide (17.5 mL) and deionized water (137.5 mL) were added to the reaction mixture and continued stirring until the color turned from dark brown to bright yellowish. The bright yellow color is a strong indicator of the formation of GO from graphite. In order to remove acid and other unreacted impurities from GO surface, GO was washed three times with 1 M HCl aqueous solution, and further repeatedly washed with deionized water until a pH of 4-5 was obtained. The separation of the washed GO from solution was carried out using a centrifuge (10,000 g force) followed by dialysis. The adsorbed traces of water were removed from GO via vacuum drying over 48 hours.

The dried GO was thermally exfoliated and reduced by heating rapidly at 1000°C for 30 s (at a rate of 2000°C per minute) under nitrogen flow in a tube furnace to produce thermally reduced graphene (TRG). Furthermore, the produced TRG was dried overnight under vacuum before using in the nanocomposites.

2.2.3 Synthesis of nanocomposites via solvent blending

The TRG/PE and CB/PE composites used in this study were prepared using p-xylene solvent. A complete description of the nanocomposite synthesis methodology is reported in previous work [53].

2.2.4 Melt crystallization using differential scanning calorimetry

Melt crystallization of neat PE and its nanocomposites is studied using a modulated differential scanning calorimeter (Discovery DSC 25, TA Instruments). The standard melting and crystallization temperatures were recorded using the following procedure: about 5-10 mg sample was heated from 20°C to 140°C (higher than a melting point) at a rate of 20°C/min to remove the thermal history of the polymer. The sample was cooled from 140°C to 20°C at 5°C/min to give the standard crystallization temperature (T_c). Subsequent heating the sample from 20°C to 140°C at a rate of 5°C/min was performed to record the melting temperature (T_m).

For isothermal melt crystallization kinetics, the sample was quickly cooled to selected T_c at 60°C/m to avoid any premature crystallization after second heat and kept isothermally at fixed T_c for 10 minutes. This time was set after several trials with different samples so that all samples showed complete crystallization within this time. After complete crystallization was achieved, the sample was cooled to 20°C (equilibrium temperature) at 5°C/min, followed by heating up to 140°C at 5°C/m to record the melting point of the crystals. A similar procedure was followed for variously selected crystallization temperatures.

For the non-isothermal crystallization, protocols similar to that for isothermal crystallization were followed for the first and second heat, and during the first cooling cycle. In order to record crystallization kinetics, samples were cooled from the melting temperature in the second cycle to the equilibrium temperature (20°C) at varying cooling rates 2, 5, 10, 15 and 20°C/min, and the development of crystallization peak was recorded.

Similar protocols were repeated (isothermal and non-isothermal) for neat PE, TRG/PE, and CB/PE composites. All DSC experiments were conducted under an inert nitrogen atmosphere 50 mL/min.

2.2.5 Characterization techniques

An X'Pert3 Powder X-ray Diffractometer (XRD) from Malvern Panalytical was used to study exfoliation of graphite into TRG. The XRD scans (within 2θ range of 5-35°) were carried out at a scan speed of 0.02°/s with instrument parameters of 40 kV voltage, 20 A intensity and 1.5406 Å Cu Kα radiation.

The cryo-fractured morphology of polymer nanocomposites (gold sputter coated for 3 minutes) was studied using a JCM-5000 NeoScope Scanning electron microscope (SEM) at 15 kV.

The morphology of synthesized TRG and its dispersion in polymer nanocomposite samples were studied using transmission electron microscope (TEM) (FEI Phillips C200 at 200 kV). For TRG sheet morphology, a small amount of TRG was dispersed in acetone (0.1 mg/mL acetone) via sonication bath for 10 minutes and one drop of the dispersion was deposited on a 300-mesh Cu grid with holy carbon. For nanocomposites, samples were cut in thin slices using a diamond knife [53].

The Raman spectra were obtained using XploRA ONE confocal Raman spectrometer from Horiba Scientific. Each run war carried on with 532 nm as the excitation source and under grafting speed 1800 g/mm (focus: 10×).

2.3 Results and discussion

2.3.1 Characterization of TRG and CB

The successful oxidation of graphite into GO, followed by its exfoliation into TRG was confirmed using XRD (Figure 11). Graphite exhibited a packed, perfectly layered structure with a split intrinsic [002] peak at 2θ = 26.59°. The interlayer spacing in graphite was calculated to be ~3.44 Å using the Bragg's law ($n\lambda = 2d \sin\theta$ where λ is the wavelength of x-rays, θ is diffraction angle, and "d" is the interlayer spacing). The average particle size was estimated using the Scherrer equation [56] as follows:

$$B(2\theta)=\frac{K\lambda}{L\cos\theta} \qquad [1]$$

Here, B is full width at half maximum (FWHM), K is Scherer's constant with a value of the order of unity (here, K=0.9 [57]), L is the mean particle size and λ is the x-ray wavelength. Graphite exhibited an average particle size of about 519 Å. With oxidation, the intrinsic [002] peak of graphite shifted towards a lower 2θ value of 10.3° in GO with an interlayer spacing of 8.6 Å and average particle size of 104 Å. A small but wider [002] peak in GO is attributed to a less packed and expanded structure where the interlayer spacing is almost doubled. There was no diffraction peak observed in TRG showing a complete exfoliation of GO into graphene nanosheets.

On the other hand, CB consists of small spherically shaped carbon particles which usually do not exhibit any packed structure (no XRD peak). The CB particles generally agglomerate in the form of fractals [58] (see TEM image later).

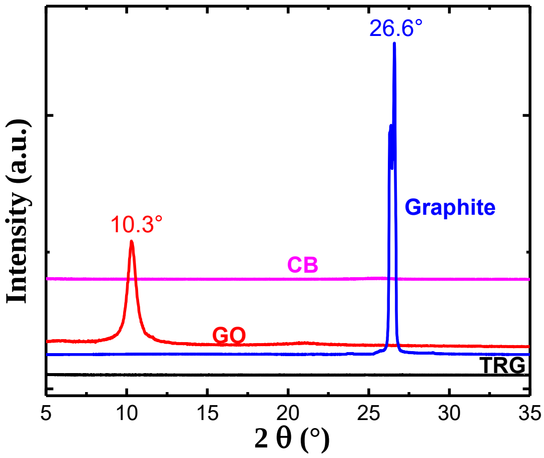

Figure 11: XRD patterns of TRG, graphite oxide, graphite, and carbon black

A paper-like morphology of graphene sheets was observed in TEM (Figure 12). The as-prepared TRG was dispersed in acetone and one drop of the suspension was dried on a TEM grid. The TEM image showed thin, wrinkled, and translucent sheets of graphene where the dark fields observed over the dark edges are attributed to the folding of nanosheets [59]. The image shows clearly separated sheets with size ~2-3 micron in the lateral dimensions. The presence of wrinkles on graphene sheets is attributed to the residual oxy-functional groups on the graphene surface [1]. On the other hand, CB particles showed considerably aggregated structures even when precipitated from highly dilute solutions. The aggregated structure shows fractals with sizes ranging to several microns [53].

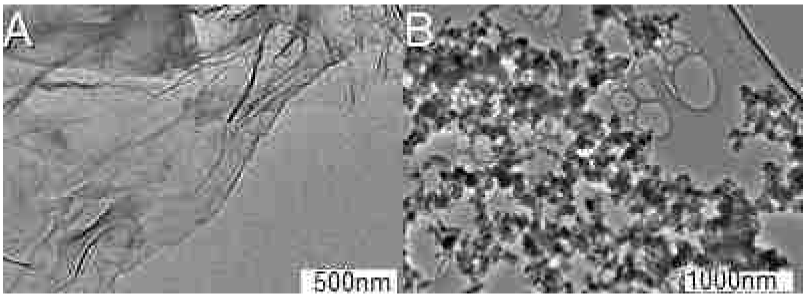

Figure 12: TEM micro-images of A) TRG and B) CB

Raman spectroscopy is a nondestructive tool to investigate structural and electronic features in graphitic materials [28]. Three pertinent pieces of information regarding the structure of graphitic materials are: 1) information about defects (D-band), 2) in-plane saturated carbon structure (G-band), and 3) the height of the stack (2D or G′-band) in the graphitic structures. The Raman spectra of graphite, CB, GO, and TRG are shown in Figure 13. The D-band showing the structural defects was observed around 1313-1400 cm^{-1}. The intensity of G-band is an indication of the stacked structure. The G-band was observed around 1550-1630 cm^{-1}. The 2D-band appears at frequency two times of that of D-band frequency and is caused by splitting in photons with opposite momentum (range of 2D-band is 2500-2800 cm^{-1}) [26]. The intensity and shape of the 2D band are used to determine the number of layers in one graphitic particle, qualitatively.

A very small D-band peak was observed in graphite whereas a large, sharp G-band peak in graphite indicated a perfectly stacked structure free from defects. The oxidation resulted in introducing defects in graphite as evident in the appearance of the D-band. However, a reduction in G-band intensity in GO is attributed to the exfoliated structure. The TRG exhibited a large change in D and G bands. The D-band increased significantly, and the G-band reduced to a value closer to the D-band intensity. The D band holds an inverse relationship between intensity and the number of graphene layers [60]. The increased defects in TRG are attributed to the thermal exfoliation method used for exfoliating GO into TRG. There was no prominent 2D band in TRG, indicating that TRG is mostly composed of single-layer graphene sheets.

In case of amorphous carbon (as TRG) an additional peak appears, called "T" peak. The T-peak appears due to the sp^3 vibration of single bonds between carbons atoms within the Raman UV excitation range (~1108 cm^{-1}) [61]. The D- and G- bands in CB appeared at the same positions as these appeared in TRG. Both materials (CB and TRG) did not show the 2D band, indicating the absence of the layered structure.

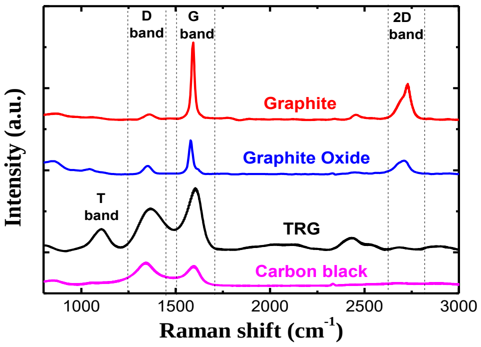

Figure 13: Raman spectra of graphite, GO, TRG, and CB

2.3.2 Morphology and dispersion in nanocomposites

The morphology of the nanocomposites was investigated SEM and TEM. Neat PE showed a smooth fractured surface (Figure 14a). The cryogenically fractured nanocomposites of PE/TRG in Figure 14c showed graphene sheets being pulled out during cryo-fracturing, heterogeneous surface with TRG. A fibrous morphology was observed for nanocomposites. The morphology of PE/CB composites was similar to that of PE/TRG nanocomposites with the difference that PE fibers were not pulled out during the cryo-fracturing.

The dispersion of graphene in PE was also studied using TEM (Figure 14b). The TEM image indicated that TRG was properly dispersed in PE with some agglomerates forming at the edges.

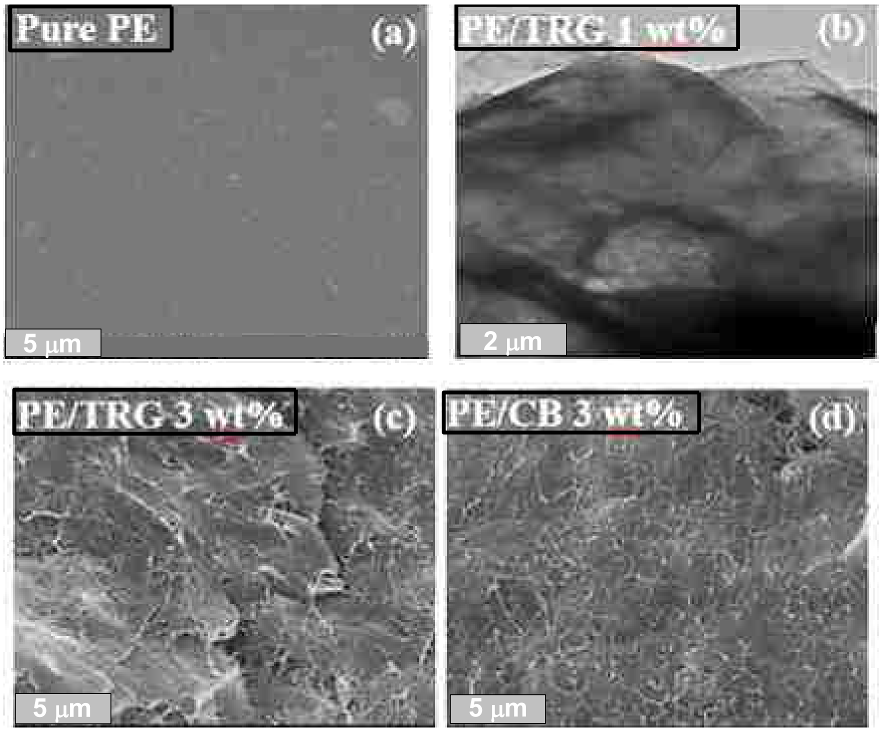

Figure 14: SEM of neat PE (a) and PE/TRG 1 wt% (b), TEM image of PE/TRG 3 wt% (c), and SEM of PE/CB 3 wt% (d)

2.3.3 Thermal characterization of nanocomposites

After eliminating the thermal history, all samples were cooled from 140°C to room temperature (20°C) at 10°C/min (same cooling rate for all samples) for recording the crystallization temperature (T_c) followed by subsequent heating scans to record the melting temperatures (T_m) at the same heating rate (10°C/min). A representative cooling (1st cycle) and heating (2nd cycle) profile of neat PE is shown in appendix. The observed T_m and T_c values for neat PE were ~122°C and ~105°C, respectively. Neat PE showed smooth transitions temperatures, showing the absence of any low molecular weight impurity in it.

The cooling and heating profiles of PE/TRG nanocomposites are shown in Figure 15 (for all composites, see the appendix). All the samples exhibited a single crystallization exotherm and a corresponding melting endotherm. The main changes observed were in the characteristic onset and peak crystallization temperatures in addition to peak broadening/stretching during crystallization. The onset temperature for crystallization increased with increasing TRG contents, attributed to the nucleating effects of TRG. The nucleation effects continued until 0.5 wt% TRG loading, which were reduced at 3 and 5 wt% TRG. A decrease in T_c at these TRG concentrations might be associated with self-agglomeration. No significant change was observed in the characteristic values of T_c and T_m with increasing TRG concentrations. This is a normal pattern shown by TRG/PE nanocomposites reported before [53].

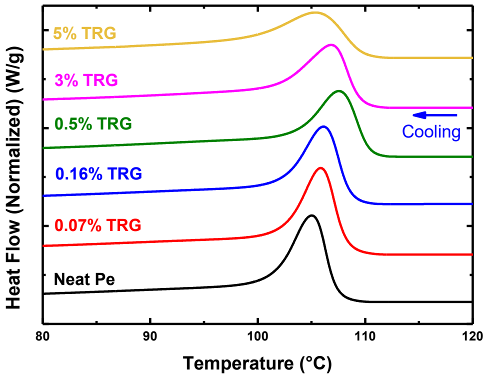

Figure 15: The cooling profiles of PE/TRG nanocomposites. (cooling = 10°C/min)

The characteristic onset, peak, and peak end temperatures for crystallization exotherms and melting endotherms are provided in Table 1. The enthalpies were calculated by integrating the area under the curves. The percentage of crystallinity in nanocomposites was calculated using the following equation:

$$X_c(\%) = \frac{\Delta H_m}{\Delta H_{100\%}(1-\theta)} \times 100\% \qquad [2]$$

Here, X_c the percentage of crystallinity of PE, ΔH_m is the melting enthalpy, $\Delta H_{100\%}$ is the melting enthalpy of a 100% crystalline PE, taken as 279 J/g[62], and θ is the mass fraction of the filler. There was no particular trend observed in Table 1 with increasing graphene concentration. However, only the onset of crystallization temperature increased with increasing graphene loading, attributed to the nucleating effects of graphene. A similar trend was observed in PE/CB composites (Table 2).

Table 1: Thermal characteristics of PE/TRG nanocomposites

PE/TRG (wt%)	**1st Cooling Scan**				**2nd Heating Scan**		
	Onset T_c (°c)	**Peak end T_c (°c)**	**Peak T_c (°c)**	**ΔH_c (J/g)**	**Peak T_m (°c)**	**ΔH_m (J/g)**	**X_c (%)**
0	107.4	34.8	105.0	101.11	122.0	93.52	33.52
0.07	108.3	32.7	104.8	104.83	121.5	94.01	33.72
0.16	108.7	34.8	106.1	100.01	121.9	91.79	32.95
0.5	110.4	31.2	107.5	103.88	122.1	95.53	34.41
3	109.6	32.9	106.8	100.4	121.8	94.26	34.83
5	109.8	34.2	105.4	94.741	122.4	85.92	32.42

Table 2: Thermal characteristics of PE/CB composites.

PE/CB (wt%)	**1st Cooling Scan**				**2nd Heating Scan**		
	Onset T_c (°c)	**Peak end T_c (°c)**	**Peak T_c (°c)**	**ΔH_c (J/g)**	**Peak end T_c (°c)**	**ΔH_m (J/g)**	**X_c (%)**
0	107.4	34.8	105.0	101.11	122.0	93.52	33.52
0.5	109.8	37.6	105.8	103.46	121.7	101.31	36.34
1.5	109.8	34.2	106.0	96.62	122.7	92.47	33.20
3	110.7	33.0	106.7	96.89	122.6	89.82	32.35
4.3	111.5	35.9	106.7	92.02	123.1	86.59	31.99
6.5	112.2	35.9	107.5	93.39	122.3	87.76	33.11
10	109.7	31.9	105.3	96.93	123.2	89.05	33.60

2.3.4 Isothermal crystallization kinetics

The isothermal crystallization kinetics of nanocomposites was investigated using DSC, and the acquired results were fitted using the Avrami equation. The isothermal crystallization is studied at four selected temperatures: 106°, 108°, 110°, and 112°C. The samples were quenched quickly from 140°C to avoid any premature crystallization before reaching the crystallization temperature [43, 63]. Following the complete crystallization at the selected temperature, the samples were cooled to equilibrium temperature at 10°C/min, and subsequently heated to 140°C at 10°C/min to record T_m associated with each crystallization temperature. Herein, crystallization data at 106°C is shown for PE/TRG and PE/CB composites whereas the rest of crystallization data is provided in the appendix.

During isothermal crystallization at 106°C, neat PE showed a small deflection at the start of crystallization attributed to premature crystallization (Figure 16). The Avrami equation, however, was applied to the major peak in PE. Increasing TRG loading shifted the crystallization peak time towards lower values, indicating the nucleation effects of TRG. A significant change was observed at 0.5 wt% TRG where the crystallization peak time was moved from 33 s for neat PE to 26.5 s for 0.5% PE/TRG nanocomposites. Increasing the amount of graphene showed adverse effects on crystallization with peak broadening at 3% graphene loading and a very broad peak at a graphene loading of 5 wt%.

A similar trend was observed in PE/CB composites. The crystallization time decreased from 27.4 s to 23.5 s as the CB loading changed from 3 wt% to 6.5 wt%. A completely distorted peak was observed at 10 wt% CB loading.

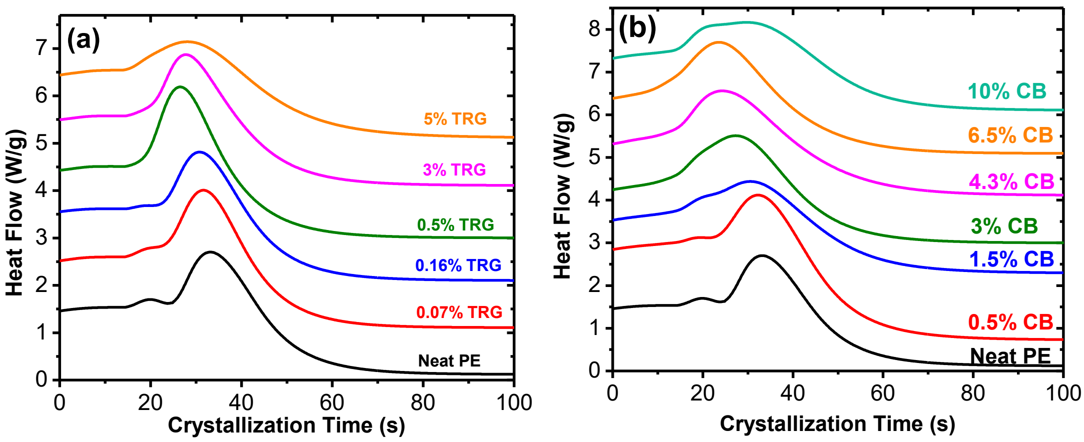

Figure 16: The isothermal crystallization of PE/TRG and PE/CB at 106°C.

The data in Figure 16 was further converted into fractional (relative) crystallinity, considering time, t_o as the onset of crystallization, and time $t-t_o$ as crystallization time (Figure 17). The relative crystallinity was calculated by dividing the maximum heat flow with the heat flow at the onset of crystallization. The data on the crystallization of selected PE/TRG nanocomposites are shown here. The remaining data can be found in appendix. The Avrami equation was used to analyze both isothermal and nonisothermal crystallization kinetics [64]. The Avrami equation is expressed as follows [42]:

$$X\left(t\right)=1-\exp\left(-kt^{n}\right) \tag{3}$$

Here, X (t) is the fraction crystallized at time t, n the Avrami index (it represents the dimensionality of the growing crystals, and predict an instantaneous or sporadic nucleation), k the overall crystallization rate constant (containing the contributions from both nucleation and growth), and t is the crystallization time in seconds [7, 42].

The experimental relative crystallinity data was fitted by using nonlinear regression with Avrami equation in order to evaluate the Avrami constants (see Table 3 for PE/TRG nanocomposites, and Table 4 for PE/CB composites). With increasing the crystallization temperature, the composites took longer time to crystallize.

The half time of crystallization ($t_{1/2}$) defined as the time required by the material to achieve 50% crystallization, is considered pertinent in understanding the crystallization kinetics. In general, a lower value of $t_{1/2}$ indicates faster crystallization. In PE/TRG nanocomposites, the experimental $t_{1/2}$ increased with increasing the crystallization temperature attributed to energetic chains which are difficult to solidify (Figure 17). On the other hand, $t_{1/2}$ decreased with increasing TRG concentration at a specific Tc. The decrease in $t_{1/2}$ can be attributed to restricted chain movement of PE in PE/TRG nanocomposites at higher loadings. In addition, $t_{1/2}$ values were also calculated from Avrami constant, k using the following expression:

$$t_{1/2} = \left(\ln 2 / k\right)^{1/n} \qquad [4]$$

An excellent agreement was observed between experimental and calculated $t_{1/2}$ values. The Avrami parameters from isothermal crystallization of PE/TRG and PE/CB nanocomposites are listed in Table 3 and Table 4, respectively.

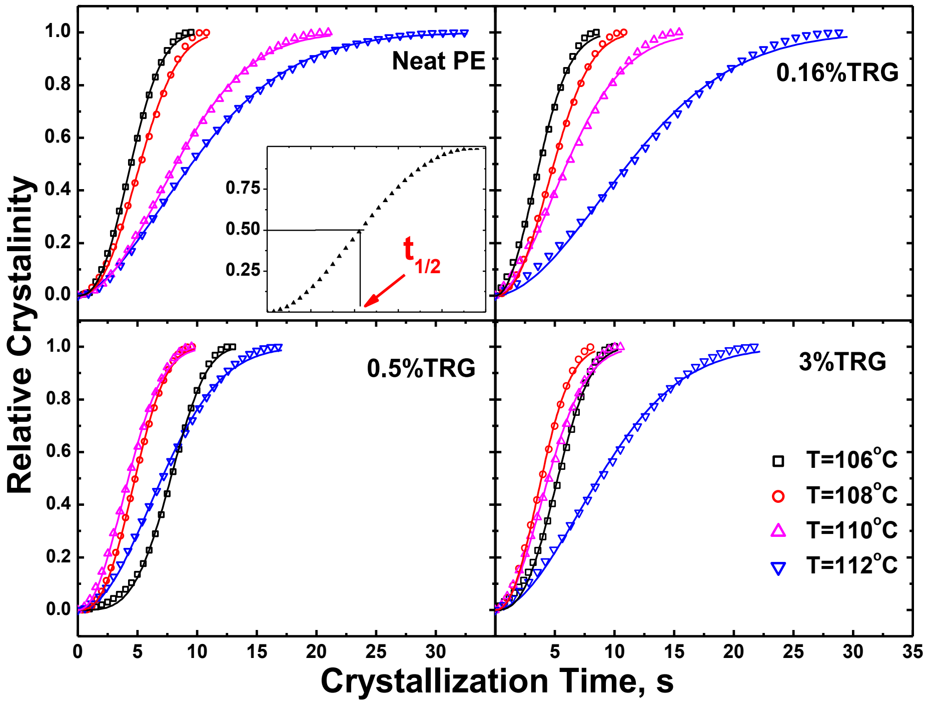

Figure 17**:** Relative crystallinity versus crystallization time for PE/TRG nanocomposites. (Marker points show experimental data and solid lines indicate Avrami fit).

The temperature dependent Lauritzen-Hoffman theory [65] represents the linear growth of crystals in polymers. According to LH theory, the growth rate of crystals during isothermal crystallization G is expressed as follows:

$$G = G_0 \exp\left(-\frac{\Delta E}{R(T_c - T_\infty)}\right)\exp\left(-\frac{K_g}{T_c \Delta T f}\right) \qquad [5]$$

Here, G_0 is a pre-exponential factor, R is the universal gas constant, ΔE is the activation energy of PE chains to the crystalline site (6276 J/mol), T_∞ is the temperature where all the motions associated with the viscous flow stop $(T_\infty = T_g - 30K = 113K)$, and T_g is the glass transition temperature for PE =143K [66]. The ΔT is the supercooling temperature, defined as $\Delta T = T_m^\circ - T_c$; T_m° is the equilibrium melting temperate for PE=395K [66], and f is the correction factor accounting for the variation of the equilibrium melting enthalpy as $f = 2T_c / (T_m^O + T_c)$. The term $\left[-\Delta E / R(T_c - T_\infty)\right]$ is used as a segmental jump rate in polymers to represent temperature dependence[67]. The factor G, representing a linear growth rate of crystals as a function of time, is defined as the inverse of the experimental crystallization $t_{1/2}$. A linear form of LH equation can be written as follows:

$$\ln G + \frac{\Delta E}{R(T_c - T_\infty)} = \ln G_0 - \frac{K_g}{T_c \Delta T f} \qquad [6]$$

The nucleation constant K_g is calculated using the following expression:

$$K_g = \frac{n b_o \sigma \sigma_e T_m^o}{k \Delta H} \qquad [7]$$

Here, n value is a function of LH theory-based crystallization regimes. The LH theory divides the crystal growth into three regimes (regime-I, regime-II, and regime-III) as a function of undercooling. The regime–I is observed when surface nuclei cause the completion of crystal growth; the regime-II represents diffusion controlled crystal growth; and regime-III represents the interfacially controlled crystal growth (similar to regime I). Thus, regimes I and III are represented by n=4 whereas regime II has n=2.

The fold surface free energy σ_e is used to understand secondary nucleation and σ is the lateral surface energy (0.0112 J/m^2 for PE); b_o is the thickness of surface monolayer (4.55 Å for PE), k is Boltzmann's constant, and ΔH is the theoretical heat of fusion (ΔH for PE = 2.8×10^8 J/m^3) [68]. The equilibrium melting temperature T_m^o was estimated using the Hoffman-Week's theory [69] (see appendix) was used to determine the equilibrium melting temperatures (T_m^o). There was a slight change in T_m^o observed in PE with the addition of TRG and CB.

For PE/TRG nanocomposites, K_g and σ_e showed a similar trend with increasing graphene concentration (Table 3). For neat PE, K_g=12640 K^2 and σ_e=6.03 kJ/m^2.K were observed. Increasing TRG concentration in PE decreased K_g to 3076 at 5 wt% TRG loading whereas σ_e decreased to a value of 1.47 at the same loading. A decreased σ_e is attributed to reduced work required to produce a new surface during the solidification process, confirming TRG as a nucleating agent for PE [70]. Similarly, these values dropped significantly when the concentration of CB was increased beyond 3 wt% in PE/CB composites (Table 4).

2.3.5 Nonisothermal crystallization kinetics

Most of the polymer processing and product-forming techniques undergo nonisothermal conditions, leading to the significance of understanding the nonisothermal crystallization behavior. The molten, history-removed samples were cooled at various cooling rates φ (2, 5, 10, 15, and 20°C/min), and the crystallization exotherms were recorded.

Table 3: Parameters summary for PE/TRG nanocomposites with increasing TRG wt%

From thermal data						Avrami Theory				LH-Theory	
TRG wt%	**T_c (°C)**	**T_m (°C)**	**T^o_m (°C)** [£]	**ΔH_m (J/g)**	**X_c %**	**$t_{1/2}^*$**	**$t_{1/2}^{**}$**	**K ($\times 10^2$)**	**n**	**K_g (K^2)**	**σ_e (kJ/m^2)**
0	106	122.2	124.0	96.1	34.5	4.4	4.5	1.68	2.5	12640	6.03
	108	122.4		95.8	34.3	5.2	5.3	1.32	2.4		
	110	122.6		95.0	34.1	8.2	8.2	1.14	2.0		
	112	122.2		96.8	34.7	9.5	9.4	1.54	1.7		
0.07	106	121.5	121.8	96.0	34.4	4.5	4.6	1.97	2.4	14178	6.81
	108	121.3		95.2	34.2	5.2	5.3	1.52	2.3		
	110	121.6		95.1	34.1	8.6	8.7	0.65	2.2		
	112	123.9		95.1	34.1	15.5	15.8	0.21	2.1		
0.16	106	121.9	121.9	91.0	32.7	3.7	3.8	4.50	2.1	12063	5.79
	108	121.8		90.1	32.4	4.9	5.0	1.77	2.3		
	110	121.9		90.0	32.3	6.0	6.2	2.80	1.8		
	112	123.3		89.0	31.9	11.1	11.4	0.86	1.8		
0.5	106	122.1	121.2	94.3	34.0	7.8	7.9	0.03	3.8	5751	2.77
	108	121.6		93.7	33.7	4.8	4.8	1.05	2.7		
	110	121.9		92.9	33.5	4.2	4.3	3.05	2.2		
	112	123.0		97.4	35.1	7	7.1	1.22	2.1		
3	106	121.9	121.0	94.3	34.9	5.2	5.4	0.74	2.7	5992	2.88
	108	121.5		93.1	34.4	3.9	3.9	3.08	2.3		
	110	121.7		92.9	34.3	4.4	4.5	3.36	2.0		
	112	123.4		92.5	34.2	8.7	8.9	1.21	1.9		
5	106	122.6	122.5	85.6	32.3	6.1	6.1	2.19	1.9	3076	1.47
	108	122.4		84.5	31.9	3.5	3.6	2.60	2.6		
	110	122.6		84.1	31.7	5.2	5.3	4.11	1.7		
	112	122.9		87.5	33.0	6.2	6.3	2.81	1.8		

[£] Calculated from Hoffman-Weeks plots using ref [69].
$t_{1/2}^*$ calculated using equation [1]
$t_{1/2}^{**}$ obtained from Figure 17

Figure 18 shows the nonisothermal crystallization behavior of the selected PE/TRG and PE/CB composites at a fixed cooling rate (10°C/min). The typical crystallization parameters such as the onset of crystallization (T_o), exothermic peak maxima (T_p), and crystallization half time ($t_{1/2}$) were obtained from these thermograms (Table 5 for PE/TRG and PE/CB nanocomposites). Increasing filler concentration increased T_o, T_p, and decreased $t_{1/2}$ for both types of the composites, attributed to heterogeneous nucleating effects of the fillers [43, 52].

Table 4: Parameters summary for PE/CB composites with increasing CB wt%

From thermal data						**Avrami Theory**				**LH-Theory**	
CB wt%	**T_c (°C)**	**T_m**	**T^o_m (°C) £**	**ΔH_m (J/g)**	**X_c %**	**$t_{1/2}^*$ (s)**	**$t_{1/2}^{**}$ (s)**	**K ($\times 10^2$)**	**n**	**K_g**	**σ_e ($\times 10^3$)**
0	106	122.2	124.1	96.1	34.5	4.4	4.5	1.68	2.5	12565	6.00
	108	122.4		95.8	34.3	5.2	5.3	1.32	2.4		
	110	122.7		95.0	34.1	8.2	8.2	1.14	2.0		
	112	122.2		94.5	33.9	9.5	9.4	1.54	1.7		
0.5	106	121.9	123.7	101.1	36.4	5.2	5.2	1.17	2.5	15641	7.47
	108	122.0		101.8	36.7	5.2	5.3	1.76	2.2		
	110	122.4		100.7	36.3	8.3	8.4	0.75	2.1		
	112	122.7		101.0	36.4	13.7	13.9	0.33	2.1		
1.5	106	122.4	124.6	93.6	34.0	4.5	4.7	2.92	2.1	14971	7.14
	108	122.6		92.7	33.7	3.0	3.0	6.84	2.1		
	110	122.9		91.7	33.4	5.6	5.7	1.62	2.2		
	112	122.7		97.9	35.6	9.4	9.4	0.72	2.0		
3	106	122.3	124.4	90.4	33.4	3.3	3.5	13.20	1.4	8152	3.89
	108	122.5		89.1	31.9	5.4	5.5	0.68	2.8		
	110	122.7		88.2	31.6	6.3	6.4	0.15	3.4		
	112	122.4		96.3	34.5	5.8	5.9	0.27	3.2		
4.3	106	122.9	123.3	88.9	33.3	6.0	6.1	0.93	2.4	-6408	-3.07
	108	122.9		86.6	32.4	4.7	4.6	1.73	2.4		
	110	123.0		85.7	32.1	3.1	3.1	7.56	2.0		
	112	123.5		90.4	33.9	3.5	3.6	4.72	2.1		
6.5	106	121.9	123.3	87.4	33.5	5.3	5.5	2.47	2.0	-5558	-2.66
	108	122.0		86.9	33.3	3.8	4.0	4.55	2.0		
	110	122.2		86.5	33.2	2.8	2.8	10.64	1.8		
	112	122.1		91.6	35.1	3.3	3.4	5.91	2.1		
10	106	123.0	124.8	89.1	35.5	5.7	5.7	0.70	2.6	-9299	-4.43
	108	123.2		87.7	34.9	4.4	4.4	1.32	2.7		
	110	123.4		86.0	34.2	2.6	2.7	10.92	1.9		
	112	123.0		94.0	37.4	3.1	3.2	6.22	2.1		

£ Calculated from Hoffman-Weeks plots using ref [69].

$t_{1/2}^*$ calculated using equation [1]

$t_{1/2}^{**}$ obtained from Figure 17

For example, increasing graphene concentration in PE/TRG nanocomposites from 0 (neat PE) to 0.5 wt% increased peak temperature, T_P from 105.7°C to 107.9°C, respectively, which decreased to a value of 105.5°C at 5 wt% loading. The increase in T_P with the addition of TRG indicates expectedly increased nucleation and formation of a thicker interface [52]. On the other hand, a peak value of T_P=108.1°C was observed for PE/CB composites which reduced to 106°C at 10 wt% CB concentration.

Similar trends were observed for T_o and $t_{1/2}$ for both types of nanocomposites (see Table 5).

Furthermore, increasing φ decreased the peak crystallization temperature for all samples (Table 5), attributed to low-temperature nucleation of the crystallites at higher cooling rates [52]. Higher the cooling rate, restricted are the molecules leading to decreased nucleation because the system reaches a lower temperature before nuclei could emerge. The enthalpy of crystallization (ΔH_c) (calculated from the area under the crystallization curve) is a direct indication of percentage crystallinity also decreased with increasing the filler concentration as well as increasing the cooling rate (see Table 5). Increasing the cooling rate provides less time for nucleation leading to less enthalpy required to crystallize [52, 70].

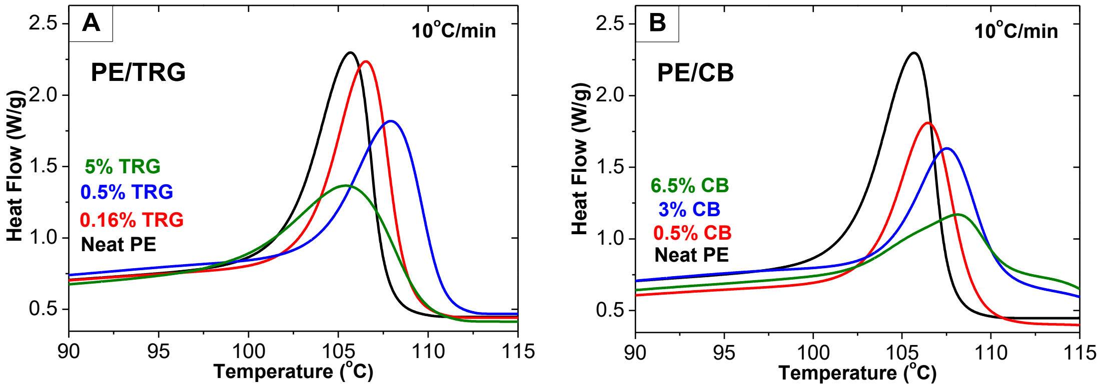

Figure 18: Nonisothermal crystallization thermograms of selected samples A) PE/TRG, B) PE/CB (Cooling rate = 10°C/min)

The nonisothermal crystallization data (which is a function of temperature) can be converted into relative crystallinity versus time using the following equation [71]:

$$t = \frac{T_o - T}{\varphi} \qquad [8]$$

Figure 19 shows relative crystallinity versus temperature for the selected PE/TRG nanocomposites and the corresponding time-converted crystallinity. The $t_{1/2}$

calculated at 50% of crystallization from the onset point, decreased with increasing the cooling rate. Furthermore, the apparent $t_{1/2}$ for neat PE decreased with increasing graphene concentration in the nanocomposites. The $t_{1/2}$ decreased with instant TRG addition (see Table 5) confirming the nucleating characteristics of graphene. On the other hand, there were no significant changes in $t_{1/2}$ for PE/CB composites as expected.

Table 5: Thermal characteristics nanocomposites from nonisothermal crystallization experiments

TRG wt%	**φ** (°C/min)	**T_o** (°C)	**T_p** (°C)	**$t_{1/2}$** (s)	**ΔH_c** (J/g)	**CB wt%**	**φ** (°C/min)	**T_o** (°C)	**T_p** (°C)	**$t_{1/2}$** (s)	**ΔH_c** (J/g)
0	2	112.7	110.0	80.9	114.2	**0.5**	2	114.7	111.0	155.8	97.4
	5	111.0	107.8	32.8	106.0		5	113.1	108.7	65.3	93.3
	10	108.3	105.7	15.3	104.8		10	110.3	106.5	34.7	90.2
	15	106.8	104.2	9.5	103.2		15	109.1	104.9	24.1	88.8
	20	105.9	103.0	6.4	101.0		20	108.1	103.6	20.6	87.6
0.07	2	113.5	110.5	95.8	112.7	**1.5**	2	115.7	111.4	177.2	109.0
	5	112.0	108.3	36.6	115.4		5	113.4	108.9	84.7	100.5
	10	110.0	106.3	19.4	111.6		10	111.3	106.4	48.5	96.3
	15	108.5	104.8	12.8	106.6		15	109.7	104.6	33.9	95.2
	20	108.0	103.6	9.4	106.7		20	108.8	103.1	26.2	95.0
0.16	2	114.1	110.9	77.8	119.0	**3**	2	117.2	112.0	174.4	106.5
	5	112.1	108.7	32.7	109.4		5	114.5	109.7	85.2	101.9
	10	110.3	106.6	17.2	105.9		10	112.8	107.5	49.5	98.0
	15	108.5	105.1	11.3	104.3		15	111.2	106.0	37.8	96.4
	20	107.6	103.9	8.3	103.9		20	109.6	104.7	27.1	96.1
0.5	2	115.2	112.4	41.3	78.0	**4.3**	2	116.1	111.9	198.3	112.2
	5	113.6	110.3	24.1	110.0		5	114.7	109.8	90.1	102.4
	10	111.9	107.9	11.4	107.2		10	113.3	107.5	51.9	99.0
	15	110.5	106.3	9.9	104.4		15	111.5	106.0	37.3	96.5
	20	109.1	105.0	7.6	103.6		20	110.0	104.6	30.0	94.6
3	2	114.7	111.5	55.9	65.0	**6.5**	2	117.0	112.2	155.6	74.1
	5	112.8	109.1	30.4	98.2		5	115.7	110.2	82.6	93.6
	10	110.6	106.8	16.5	97.6		10	113.6	108.1	47.0	91.6
	15	109.6	105.0	11.2	96.9		15	112.5	106.6	33.4	90.3
	20	108.1	103.6	8.1	96.7		20	111.6	105.1	25.9	89.9
5	2	114.7	111.0	54.6	66.8	**10**	2	114.4	111.1	173.0	106.5
	5	112.9	108.4	32.0	101.4		5	112.6	108.6	80.6	100.0
	10	111.2	105.5	19.2	98.0		10	110.4	106.0	46.2	96.4
	15	109.4	103.2	13.5	95.2		15	109.2	104.1	32.2	94.0
	20	108.2	101.4	10.7	94.0		20	107.9	102.6	24.8	93.6

2.3.5.1 Analysis of nonisothermal crystallization kinetics

The evolution of crystallinity during nonisothermal crystallization was also studied using the Avrami, Ozawa, and Liu’s kinetic models. These models are used to understand the structure development during the course of the crystallization under nonisothermal conditions. The following sections contain an analysis of nonisothermal crystallization data using the above-mentioned theories.

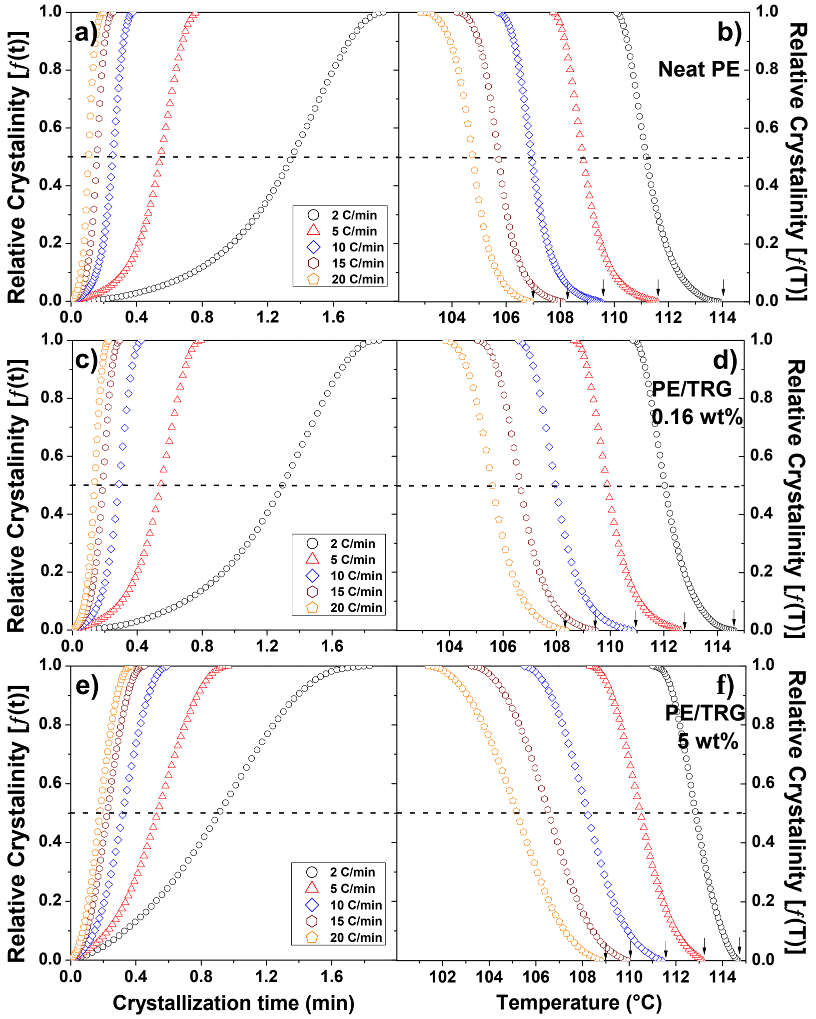

Figure 19: Relative crystallinity versus crystallization time and temperature. (The dotted line indicates 50% of crystallization during the evolution of crystallinity. The arrow signs in right panels indicate the onset of crystallization temperatures).

2.3.5.2 Avrami analysis

The Avrami equation is traditionally developed for isothermal crystallization of polymers. In order to evaluate the nonisothermal crystallization data using the Avrami equation, the relative crystallinity was converted from temperature variable to time variable [71]. Using the time variation, the nonisothermal kinetic data can be treated by the methods used for isothermal kinetic analysis. However, Jeziorny [72] proposed a correction factor called as the corrected crystallization rate for nonisothermal crystallization (k_c) to replace the Avrami crystallization rate as follows:

$$\log k_c = \frac{\log k}{|\varphi|} \quad [9]$$

The Jeziory's correction follows that the crystallization rate should be adjusted to accommodate a constant cooling rate experiment [72]. The time-dependent nonisothermal crystallization data was fitted with the linearized Avrami equation (Figure 20) and a summary of the results are shown in Table 6. The data exhibited an excellent fit with the Avrami equation.

The kinetic parameters, n, and k for neat PE, PE/TRG, and PE/CB composites are presented in Table 6. The table shows a similar pattern to what was shown by Liu [73]. The Avrami exponent, n is related to the type of the nucleation and growth geometry of the crystals. Although the Avrami exponent does not define a unique nucleation and growth process, there is a possibility that a relationship can be made between the n value, the crystallization mechanisms, and the morphology and structure in the crystalline state [40]. On average, an exponent of 1.6 for neat PE crystallized at all temperatures is consistent with the two-dimensional spherical crystal growth process. With the addition of 0.07 wt% TRG, n value reduced to 1.4, 1.6 at 0.5 wt% TRG, and reduced to 1.4 at 5 wt% TRG. Although the assumptions used to derive the Avrami equation should result in n being integer values for the homogenous nucleation and linear growth processes, the non-integer value could be expected in heterogeneous nucleation processes due to mixed nucleation modes [74]. In general, along with excellent Avrami fit, the n value in the range of 1-2 indicated two-dimensional growth PE/TRG nanocomposites. The PE/CB composites showed similar behavior with n hitting the lower end of the same range (closer to a value of 1).

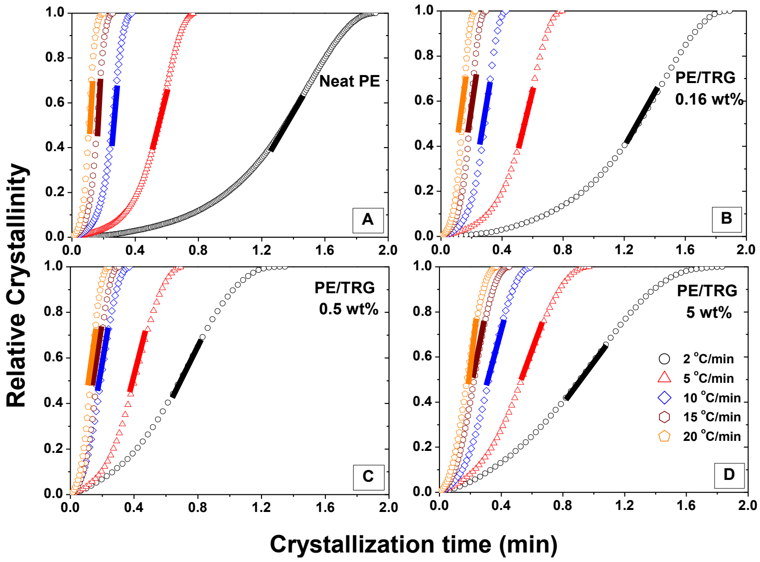

Figure 20: Effect of cooling rates on the crystallization of PE/TRG nanocomposites. [Marker points represent experimental data and smooth lines the Avrami fit].

2.3.5.3 Ozawa’s theory

The Ozawa’s crystallization theory assumes crystallization occurs at a constant rate and the crystals grow from an initial distribution of the nuclei in the form of spherulites (three-dimensional crystals with a constant growth radius at a given temperature) [44]. Ozawa’s theory further assumes that the crystallization process is essentially a result of small isothermal crystallization steps. The temperature-dependent relative crystallinity, X (T), is a function of the cooling rate (φ), represented as follows[IX] [45]:

$$1 - X\left(T\right) = \exp\left(-k(T)/\varphi^{n}\right) \qquad [10]$$

Here, k (T) is the crystallization rate constant (function of temperature), and n=m+2 where m is the Ozawa’s parameter which is a function of dimensions of the crystal growth and nucleation mechanism. The linearized Ozawa’s equation is represented as follows[X]:

$$\log\left[-\ln\left(1-X\left(T\right)\right)\right]=\log K\left(T\right)-n\log\varphi \qquad [11]$$

Table 6: Avrami parameters of nonisothermal crystallization of the composites.

TRG wt%	Avrami constant				CB wt%	Avrami constant		
	φ	n	k_c (min) (10)	R^2		n	k_c (min) (10)	R^2
0	2	2.0	4.1	0.998	0.5	1.0	10.6	0.999
	5	1.2	7.5	0.996		1.0	12.3	1.000
	10	1.5	10.2	0.993		1.2	16.4	0.998
	15	1.8	11.3	0.993		1.0	21.3	1.000
	20	1.7	11.2	0.994		1.0	27.8	0.998
0.07	2	1.4	2.2	0.996	1.5	1.1	10.3	1.000
	5	1.2	7.5	0.998		1.1	12.3	1.000
	10	1.3	9.5	0.997		1.0	16.2	1.000
	15	1.5	10.4	0.994		1.0	21.2	1.000
	20	1.4	10.4	0.997		1.1	27.7	1.000
0.16	2	2.1	4.6	0.996	3	1.4	10.6	0.997
	5	1.2	7.7	0.999		1.1	12.3	1.000
	10	1.4	9.9	0.995		1.2	16.4	0.999
	15	1.7	10.9	0.994		1.3	21.3	0.999
	20	1.5	10.7	0.996		1.2	27.8	0.999
0.5	2	1.5	8.9	0.995	4.3	1.5	11.0	0.993
	5	1.3	9.4	0.995		1.2	12.7	0.999
	10	1.6	11.9	0.995		1.2	17.2	0.998
	15	1.8	11.5	0.993		1.3	21.6	0.998
	20	1.6	11.1	0.996		1.2	28.1	0.999
3	2	1.7	7.4	0.998	6.5	1.7	10.8	0.994
	5	1.2	8.4	0.998		1.3	12.5	0.999
	10	1.4	10.3	0.995		1.2	16.6	0.997
	15	1.7	11.1	0.994		1.3	21.4	0.998
	20	1.5	10.9	0.997		1.2	28.0	0.999
5	2	1.6	8.0	0.999	10	1.0	10.9	1.000
	5	1.1	8.6	0.999		1.0	12.6	0.997
	10	1.4	10.2	0.997		0.9	16.6	0.999
	15	1.5	10.8	0.996		0.9	21.7	0.999
	20	1.4	10.6	0.998		1.0	28.3	1.000

Fitting the experimental data into linearized Ozawa’s equation was attempted and values of k (T) and m were evaluated from the slope and intercept of the straight lines, respectively. The straight lines were obtained at selected temperatures (Figure

21). The average values of the Ozawa's constant were 3.7, 2.7, 2.8, 2.4, 3.4, and 1.7 for neat PE, 0.07 wt%, 0.16 wt%, 0.5 wt%, 3 wt%, and 5 wt% PE/TRG nanocomposites, respectively. Higher values of m were expected compared to averaged values of the Avrami exponent [64]. Similarly, the averaged m decreased from 1.7 at 0.5 wt% PE/CB to 1.1 at 10 wt% PE/CB composites. An m value of ~2-3 corresponds to instantaneous nucleation and growth of spheres in 3D [64]. The Ozawa's analyses were applied to all composite samples (see appendix). However, PE/TRG nanocomposites showed excellent agreement with Ozawa's theory whereas PE/CB composites did not show very good fittings. A few previous reports [75, 76] also indicated unsuccessful fitting of the Ozawa equation in PE-based composites. One of the possible reasons for crystallization not following Ozawa's approach might be the strong presence of secondary crystallization mechanism which is also evident from the Avrami analysis.

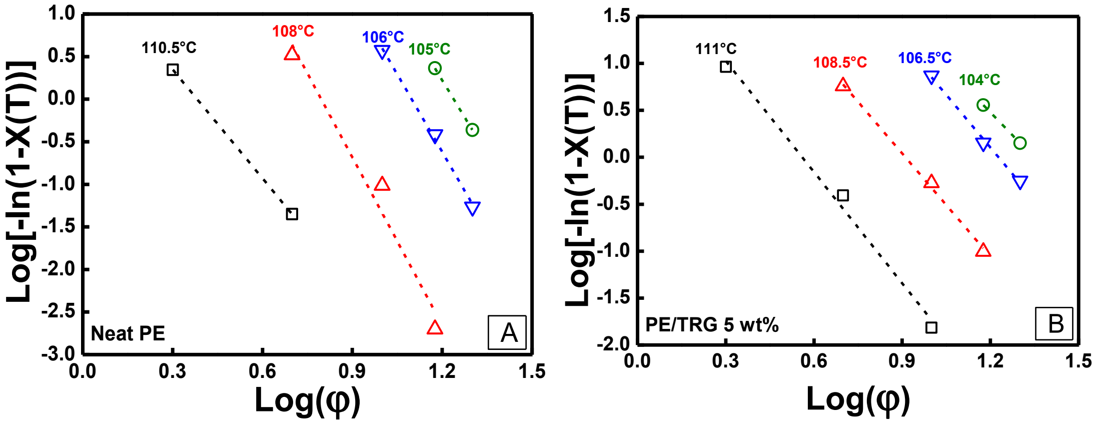

Figure 21: Representative Ozawa plots of selected samples A) Neat PE, B) PE/TRG 5 wt%

2.3.5.4 Liu's analysis

A crystallization equation developed by Liu et al. [77] combines the Ozawa and Avrami equations to describe the nonisothermal crystallization kinetics. The applicability of Liu equation has been reported for crystallization of various kinds of nanocomposite systems [45, 73, 76]. It represents a relationship between the cooling rate, φ and time, t, at fixed levels of crystallinity as follows:

$$\varphi = \frac{\left[k(T)/k\right]^{\frac{1}{m}}}{t^a} = \frac{F\left(T\right)}{t^a} = F\left(T\right)t^{-a} \qquad [12]$$

$$\log\varphi = \log F\left(T\right) - a\log t \qquad [13]$$

Here, a is the ratio of the Avrami's exponent "n" to the Ozawa's exponent "m" (i.e. a=n/m), the term $[k(T)/k]^{1/m}$ represents the value of cooling/heating rate at a certain degree of crystallinity (for simplicity, it is equal to F (T)).

Using linear regression again, the exponent "ɑ" and F(T) were estimated at fixed % crystallinity (Figure 22). The data did not fit perfectly with Liu's model. However, the trend of F(T) as a function of W_c% was the same as reported earlier for polyamide/graphene oxide nanocomposites [78]. The value of F (T) increased with increasing W_c (Table 8), indicating that a lower crystallization rate is required to reach a certain degree of crystallinity at a set time. On the other hand, the exponent "ɑ" which is the ratio of the Avrami to Ozawa's constants did not yield a proper value. This negativity was shown for the first time and we could not explain it. Similar behavior was observed for PE/CB composites (see appendix).

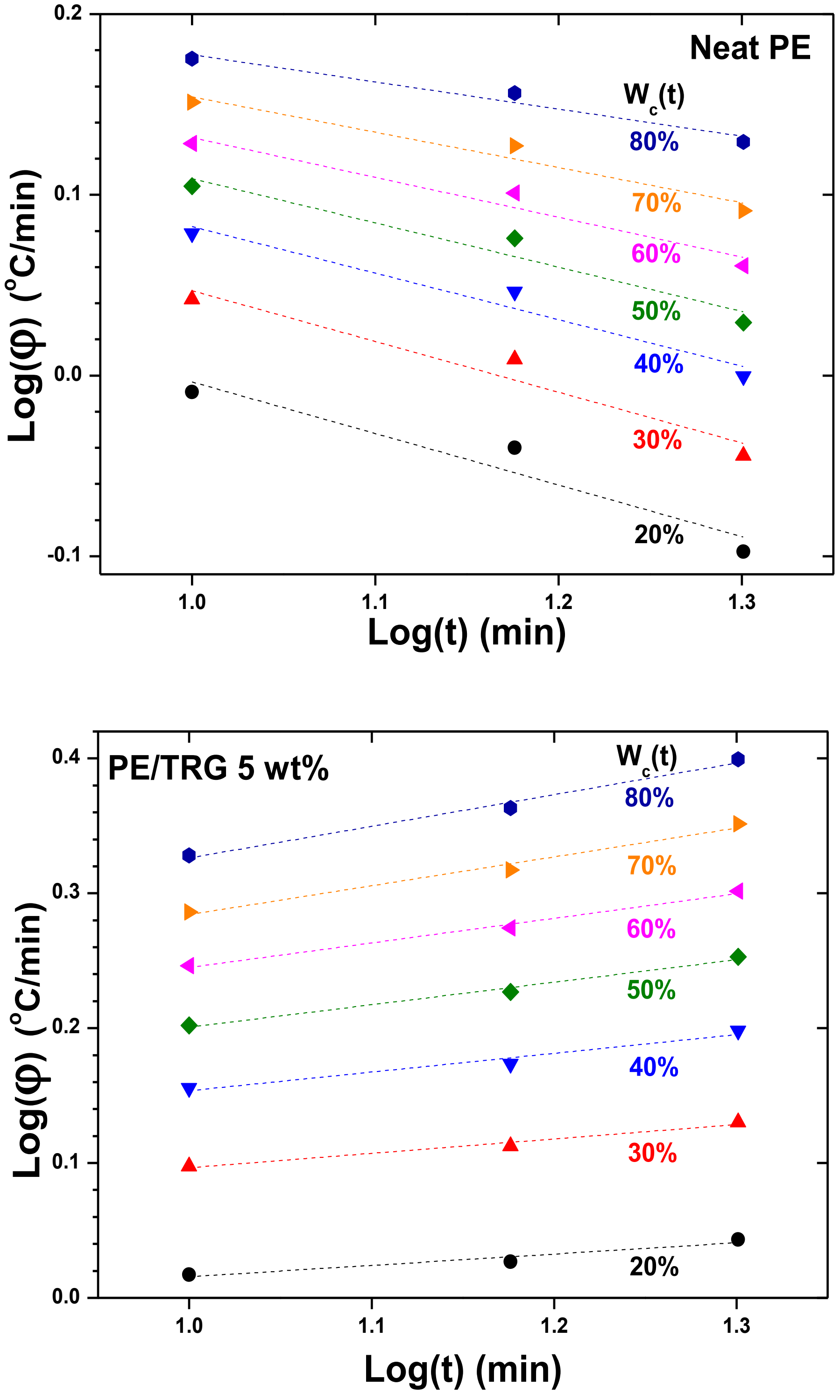

Figure 22: Liu’s plot for Neat PE and PE/TRG nanocomposites

Table 7: Liu's theory parameters for nanocomposites

TRG wt%	**W_c (t)%**	**F(T)**	**a**	**R^2**	**CB w%**	**W_c (t)%**	**F(T)**	**a**	**R^2**
0	20	1.9	0.3	0.857	**0.5**	20	2.0	-0.1	0.955
	30	2.1	0.3	0.895		30	2.2	-0.1	0.956
	40	2.2	0.3	0.919		40	2.4	-0.1	0.956
	50	2.3	0.2	0.894		50	2.5	-0.1	0.955
	60	2.2	0.2	0.917		60	2.6	-0.1	0.947
	70	2.2	0.2	0.912		70	2.7	-0.1	0.950
	80	2.1	0.2	0.924		80	2.8	-0.1	0.941
0.07	20	1.5	0.1	0.890	**1.5**	20	2.0	-0.2	1.000
	30	1.6	0.1	0.848		30	2.3	-0.2	1.000
	40	1.7	0.1	0.896		40	2.4	-0.2	1.000
	50	1.8	0.0	0.582		50	2.6	-0.2	1.000
	60	1.9	0.0	0.644		60	2.7	-0.2	1.000
	70	2.0	0.0	0.852		70	2.8	-0.2	1.000
	80	2.0	0.0	0.786		80	2.9	-0.2	1.000
0.16	20	1.3	0.1	0.878	**3**	20	1.6	-0.3	1.000
	30	1.5	0.1	0.943		30	2.1	-0.2	1.000
	40	1.6	0.1	0.833		40	2.3	-0.2	1.000
	50	1.7	0.1	0.916		50	2.5	-0.2	1.000
	60	1.7	0.0	0.849		60	2.6	-0.2	1.000
	70	1.7	0.0	0.945		70	2.8	-0.2	1.000
	80	1.8	0.0	0.360		80	2.9	-0.2	1.000
0.5	20	0.2	-0.5	0.665	**4.3**	20	1.2	-0.3	0.998
	30	0.2	-0.5	0.695		30	2.6	-0.2	0.977
	40	0.3	-0.5	0.732		40	2.8	-0.2	0.981
	50	0.4	-0.4	0.716		50	2.9	-0.2	0.977
	60	0.4	-0.4	0.747		60	3.1	-0.2	0.975
	70	0.5	-0.4	0.803		70	3.2	-0.2	0.975
	80	0.5	-0.4	0.809		80	3.3	-0.2	0.974
3	20	1.1	0.1	-0.023	**6.5**	20	0.5	-0.5	0.963
	30	1.3	0.0	-0.081		30	0.7	-0.4	0.980
	40	1.4	0.0	-0.341		40	1.2	-0.4	0.977
	50	1.4	0.0	-0.488		50	2.2	-0.3	0.965
	60	1.5	0.0	-0.967		60	2.4	-0.3	0.962
	70	1.5	0.0	-0.144		70	2.6	-0.2	0.965
	80	1.5	0.0	0.511		80	2.8	-0.2	0.967
5	20	0.9	-0.1	0.877	**10**	20	2.1	-0.2	0.996
	30	1.0	-0.1	0.959		30	2.3	-0.2	0.997
	40	1.0	-0.1	0.932		40	2.4	-0.2	0.996
	50	1.1	-0.2	0.974		50	2.5	-0.2	0.996
	60	1.2	-0.2	0.985		60	2.7	-0.2	0.995
	70	1.2	-0.2	0.969		70	2.8	-0.2	0.995
	80	1.2	-0.2	0.978		80	2.9	-0.2	0.995

Chapter 3: Conclusions and Future Recommendation

3.1 Conclusions

In this study, thermally reduced graphene (TRG) was successfully synthesized by simultaneous thermal exfoliation and reduction of graphite oxide. TRG was confirmed vie XRD, Raman spectroscopy, and TEM. PE/TRG and PE/CB composites were prepared using solvent blending at a varying concentration of the fillers.

The isothermal data was an excellent fit with the Avrami model with Avrami exponent ranging 2-3 (non-integer values), attributed to heterogeneous crystallization of PE chains on TRG surface. The half time of crystallization ($t_{1/2}$) decreased with increasing graphene concentration confirming graphene as a nucleating agent. The Lauritzen-Hoffman treatment of the crystallization data indicated a reduction in energy required to crystallize with increasing filler concentrations (for both TRG and CB). The surface energy dropped from 6.03 for neat PE to 1.47 for 5 wt% TRG and to a value of -4.43 kJ/m^2 at 10 wt% CB (Figure 23).

During nonisothermal crystallization, the peak crystallization temperature (T_p) increased with increasing TRG concentration up to percolation followed by a decrease with further increasing TRG concentration. The peak shift was attributed towards the change in the structure after composites were formed. The enthalpy of crystallization decreased with the increased cooling rate at all concentrations. The $t_{1/2}$ decreased with the increased cooling rate. Furthermore, the nonisothermal data was an excellent fit to the modified Avrami equation and Ozawa model whereas the Liu models did not provide a good fit. With increasing filler concentration, crystals grew from as one-dimensional rods with an instantaneous growth as predicted by the Avrami theory.

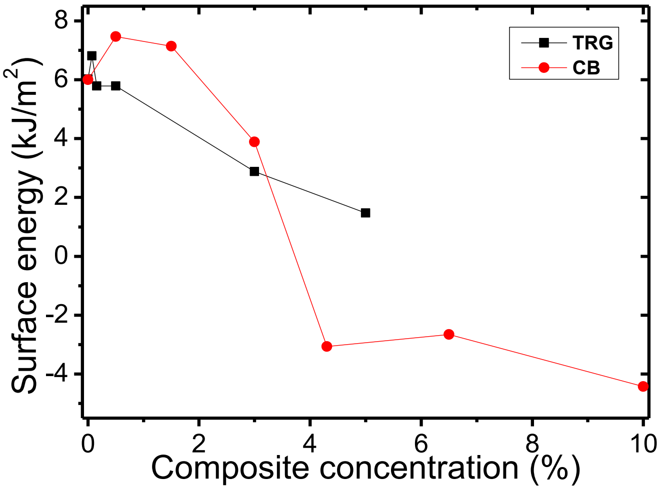

Figure 23: the change in the surface energy vs composite concentration.

3.2 Future recommendations

The vast area of application of polymer nanocomposites gives it many opportunities for future works. During the course of this thesis, many ideas came up to give additional aid to reveal the science behind polyethylene/graphene nanocomposites. Due to the time limitation, these ideas were not performed.

3.2.1 Kinetics confirmation

As it was shown before, the Avrami exponent ranged between 2-3 (disc to Sphere crystallization shape). Due to the time constraints, we were unable to support the theoretical developments with experimental evidence. One of the instruments that can provide this experimental confirmation is the wide-angle X-ray scattered (WAXS). The WAXS instrument is quite common in the crystallization area due to the ability to monitor the change in crystal length under time-resolved experiments [79]. Another experimental proof can be obtained by studying the crystallization behavior vie optical microscopy under heating-cooling cycles.

3.2.2 Additional tests

Due to the instrument’s limitation, the effect of adding the graphene to the polyethylene on glass transition could not be conducted. Since the glass transition temperature of polyethylene requires an extreme cooling experiment (-130ºC [7]), a more advanced instrument is required to investigate this region. Fast scanning calorimetry (FSC) is more recent and advanced scanning calorimetry can achieve a wide range of heating/cooling rates. In addition, to studying the glass transition, FSC can provide overcritical cooling and generation of amorphous glassy states[80].

References

[1] M. Z.Iqbal, "Structure-property relationships in graphene/polymer nanocomposites," PhD Thesis, Chemical Engineering, Colorado School of Mines. Arthur Lakes Library, Colorado School of Mines. Arthur Lakes Library, 2016.

[2] N. B. Hannay, *Treatise on Solid State Chemistry: Volume 3 Crystalline and Noncrystalline Solids*, 1976.

[3] L. J. Smith, K. M. Fiebig, H. Schwalbe, and C. M. Dobson, "The concept of a random coil: Residual structure in peptides and denatured proteins," *Folding and Design,* vol. 1, pp. R95-R106, 1996.

[4] V. P. Privalko, Y. S. Lipatov, and A. P. Lobodina, "Surface tension, density, and viscosity in chain-folded polymer melts," *Journal of Macromolecular Science, Part B,* vol. 11, pp. 441-454, 1975.

[5] G. S. Y. Yeh, "Order in amorphous polystyrenes as revealed by electron diffraction and diffraction microscopy," *Journal of Macromolecular Science, Part B,* vol. 6, pp. 451-463, 1972.

[6] W. Pechhold, M. E. T. Hauber, and E. Liska, "The meander model of condensed polymers," *Kolloid-Zeitschrift und Zeitschrift für Polymere,* vol. 251, pp. 818-828, 1973.

[7] L. H. Sperling, *Introduction To Physical Polymer Science*, 4th ed. Hoboken, N.J: Wiley, 2006.

[8] L. Mandelkern, *Crystallization of polymers. Volume 1, Equilibrium concepts*, First ed.: Cambridge University Press, 2002.

[9] D. C. Yang and E. L. Thomas, "An electron microscopy and X-ray diffraction study of the microstructures of melt-drawn polyethylene films," *Journal of Materials Science,* vol. 19, pp. 2098-2110, 1984.

[10] P. H. Till Jr, "The growth of single crystals of linear polyethylene," *Journal of Polymer Science,* vol. 24, pp. 301-306, 1957.

[11] M. C. Righetti, "Amorphous Fractions of Poly(lactic acid)," vol. 279, pp. 195-234, 2017.

[12] J. E. Mark, *Physical properties of polymers handbook* vol. 1076: Springer, 2007.

[13] B. P. Grady, "Effects of carbon nanotubes on polymer physics," *Journal of Polymer Science Part B: Polymer Physics,* vol. 50, pp. 591-623, 2012.

[14] X. Zhao, L. Lv, B. Pan, W. Zhang, S. Zhang, and Q. Zhang, "Polymer-supported nanocomposites for environmental application: A review," *Chemical Engineering Journal,* vol. 170, pp. 381-394, 2011.

[15] J. H. Koo, *Polymer nanocomposites*, 1 ed.: McGraw-Hill Professional Pub., 2006.

[16] T. Masciangioli and W.-X. Zhang, "Peer reviewed: environmental technologies at the nanoscale," ed: ACS Publications, 2003, pp. 102A-108A.

[17] K.-t. Lau, C. Gu, and D. Hui, "A critical review on nanotube and nanotube/nanoclay related polymer composite materials," *Composites Part B: Engineering,* vol. 37, pp. 425-436, 2006.

[18] R. Sengupta, M. Bhattacharya, S. Bandyopadhyay, and A. K. Bhowmick, "A review on the mechanical and electrical properties of graphite and modified graphite reinforced polymer composites," *Progress in Polymer Science,* vol. 36, pp. 638-670, 2011.

[19] G. Tibbetts, M. Lake, K. Strong, and B. Rice, "A review of the fabrication and properties of vapor-grown carbon nanofiber/polymer composites," *Composites Science and Technology,* vol. 67, pp. 1709-1718, 2007.

[20] M. J. Allen, V. C. Tung, and R. B. Kaner, "Honeycomb Carbon: A Review of Graphene," *Chemical Reviews,* vol. 110, pp. 132-145, 2010.

[21] L. Zhang and M. Fang, "Nanomaterials in pollution trace detection and environmental improvement," *Nano Today,* vol. 5, pp. 128-142, 2010.

[22] H. Klefenz, "Nanobiotechnology: From Molecules to Systems," *Engineering in Life Sciences,* vol. 4, pp. 211-218, 2004.

[23] F. Bonaccorso, Z. Sun, T. Hasan, and A. C. Ferrari, "Graphene photonics and optoelectronics," *Nature Photonics,* vol. 4, pp. 611-622, 2010.

[24] A. K. Geim and K. S. Novoselov, "The rise of graphene," in *Nanoscience and Technology,* ed: Co-Published with Macmillan Publishers Ltd, UK, 2009, pp. 11-19.

[25] H. Kim, A. Abdala, and C. Macosko, "Graphene/Polymer Nanocomposites," *Macromolecules,* vol. 43, pp. 6515-6530, 2010.

[26] A. C. Ferrari, "Raman spectroscopy of graphene and graphite: Disorder, electron–phonon coupling, doping and nonadiabatic effects," *Solid State Communications,* vol. 143, pp. 47-57, 2007.

[27] T. Ramanathan, A. Abdala, S. Stankovich, D. Dikin, M. Herrera-Alonso, R. Piner*, et al.*, "Functionalized graphene sheets for polymer nanocomposites," *Nature nanotechnology,* vol. 3, pp. 327-331, 2008.

[28] A. C. Ferrari and D. M. Basko, "Raman spectroscopy as a versatile tool for studying the properties of graphene," *Nat Nanotechnol,* vol. 8, pp. 235-46, Apr 2013.

[29] K. S. Novoselov, D. Jiang, F. Schedin, T. J. Booth, V. V. Khotkevich, S. V. Morozov*, et al.*, "Two-dimensional atomic crystals," *Proc Natl Acad Sci U S A,* vol. 102, pp. 10451-10453, 2005.

[30] Y. Zhang, J. P. Small, W. V. Pontius, and P. Kim, "Fabrication and electric-field-dependent transport measurements of mesoscopic graphite devices," *Applied Physics Letters,* vol. 86, pp. 073104-073106, 2005.

[31] L. R. Bunnell, "Method for producing thin graphite flakes with large aspect ratios," United States Patent, Sponsor Org, 1993.

[32] S. N. Tripathi, G. S. S. Rao, A. B. Mathur, and R. Jasra, "Polyolefin/graphene nanocomposites: a review," *RSC Advances,* vol. 7, pp. 23615-23632, 2017.

[33] A. Tchernook, M. Krumova, F. J. Tölle, R. Mülhaupt, and S. Mecking, "Composites from Aqueous Polyethylene Nanocrystal/Graphene Dispersions," *Macromolecules,* vol. 47, pp. 3017-3021, 2014.

[34] P. Liu, "Polymer modified clay minerals: A review," *Applied Clay Science,* vol. 38, pp. 64-76, 2007.

[35] Y. Lin, J. Jin, and M. Song, "Preparation and characterisation of covalent polymer functionalized graphene oxide," *J. Mater. Chem.*, vol. 21, pp. 3455-3461, 2011.

[36] M. Alberto, "Introduction of Fibre-Reinforced Polymers − Polymers and Composites: Concepts, Properties and Processes," 2013.

[37] K. Yue, G. Liu, X. Feng, L. Li, B. Lotz, and S. Z. D. Cheng, "A few rediscovered and challenging topics in polymer crystals and crystallization," *Polymer Crystallization,* vol. 1, p. e10053, 2018.

[38] I. Gutzow and J. Schmelzer, *The vitreous state: Thermodynamics, Structure, Rheology, and Crystallization*. Berlin, Heidelberg: Springer, 2013.

[39] D. Kashchiev, *Nucleation*. Sofia, Bulgaria: Elsevier, 2000.

[40] L. Mandelkern, *Crystallization of Polymers: Volume 2, Kinetics and Mechanisms*, second ed.: Cambridge University Press, 2004.

[41] G. Strobl, "Crystallization and melting of bulk polymers: New observations, conclusions and a thermodynamic scheme," *Progress in Polymer Science,* vol. 31, pp. 398-442, 2006.

[42] A. T. Lorenzo, M. L. Arnal, J. Albuerne, and A. J. Müller, "DSC isothermal polymer crystallization kinetics measurements and the use of the Avrami equation to fit the data: Guidelines to avoid common problems," *Polymer Testing,* vol. 26, pp. 222-231, 2007.

[43] E. Tarani, D. Papageorgiou, C. Valles, A. Wurm, Z. Terzopoulou, D. Bikiaris, *et al.*, "Insights into crystallization and melting of high density polyethylene/graphene nanocomposites studied by fast scanning calorimetry," *Polymer Testing,* vol. 67, pp. 349-358, 2018.

[44] T. Ozawa, "Kinetics of non-isothermal crystallization," *Polymer,* vol. 12, pp. 150-158, 1971.

[45] T. Liu, Z. Mo, and H. Zhang, "Nonisothermal crystallization behavior of a novel poly(aryl ether ketone): PEDEKmK," *Journal of Applied Polymer Science,* vol. 67, pp. 815-821, 1998.

[46] L. S. Schadler, L. C. Brinson, and W. G. Sawyer, "Polymer nanocomposites: A small part of the story," *JOM,* vol. 59, pp. 53-60, 2007.

[47] Y. Fukuyama, T. Kawai, S.-i. Kuroda, M. Toyonaga, T. Taniike, and M. Terano, "The effect of the addition of polypropylene grafted SiO 2 nanoparticle on the crystallization behavior of isotactic polypropylene," *Journal of thermal analysis and calorimetry,* vol. 113, pp. 1511-1519, 2013.

[48] R. K. Prud'Homme, I. A. Aksay, D. Adamson, and A. Abdala, "Thermally exfoliated graphite oxide," (US) Patent, 2010.

[49] M. Z. Iqbal and A. A. Abdala, "Oil spill cleanup using graphene," *Environ Sci Pollut Res Int,* vol. 20, pp. 3271-9, May 2013.

[50] C. Bao, Y. Guo, B. Yuan, Y. Hu, and L. Song, "Functionalized graphene oxide for fire safety applications of polymers: a combination of condensed phase flame retardant strategies," *Journal of Materials Chemistry,* vol. 22, pp. 23057-23063, 2012.

[51] S. Cheng, X. Chen, Y. G. Hsuan, and C. Y. Li, "Reduced Graphene Oxide-Induced Polyethylene Crystallization in Solution and Nanocomposites," *Macromolecules,* vol. 45, pp. 993-1000, 2011.

[52] Y. Fan, J. Lou, J. Jamali, Y. Lu, and J. Wood, "Effect of Clay Dispersion on the Nonisothermal and Isothermal Crystallization Behaviors of Polyethylene Composites," *Polymer-Plastics Technology and Engineering,* vol. 56, pp. 1646-1656, 2017.

[53] M. Z. Iqbal, A. A. Abdala, V. Mittal, S. Seifert, A. M. Herring, and M. W. Liberatore, "Processable conductive graphene/polyethylene nanocomposites: Effects of graphene dispersion and polyethylene blending with oxidized polyethylene on rheology and microstructure," *Polymer,* vol. 98, pp. 143-155, 2016.

[54] Z. Jin, J. R. Lomeda, B. K. Price, W. Lu, Y. Zhu, and J. M. Tour, "Mechanically Assisted Exfoliation and Functionalization of Thermally Converted Graphene Sheets," *Chemistry of Materials,* vol. 21, pp. 3045-3047, 2009.

[55] D. C. Marcano, D. V. Kosynkin, J. M. Berlin, A. Sinitskii, Z. Sun, A. Slesarev, *et al.*, "Improved Synthesis of Graphene Oxide," *ACS Nano,* vol. 4, pp. 4806-4814, 2010.

[56] B. D. Cullity, *Elements of x-ray diffraction*, 2 ed. Reading, Mass: Addison-Wesley Pub. Co, 1978.

[57] B. Saner, F. Okyay, and Y. Yürüm, "Utilization of multiple graphene layers in fuel cells. 1. An improved technique for the exfoliation of graphene-based nanosheets from graphite," *Fuel,* vol. 89, pp. 1903-1910, 2010.

[58] B. Y. Chang, N. M. Huang, M. N. An'amt, A. R. Marlinda, Y. Norazriena, M. R. Muhamad, *et al.*, "Facile hydrothermal preparation of titanium dioxide decorated reduced graphene oxide nanocomposite," *Int J Nanomedicine,* vol. 7, pp. 3379-87, 2012.

[59] M. Z. Iqbal and A. A. Abdala, "Oil spill cleanup using graphene," *Environmental Science and Pollution Research,* vol. 20, pp. 3271-3279, 2013.

[60] K. N. Kudin, B. Ozbas, H. C. Schniepp, R. K. Prud'Homme, I. A. Aksay, and R. Car, "Raman spectra of graphite oxide and functionalized graphene sheets," *Nano letters,* vol. 8, pp. 36-41, 2008.

[61] A. C. Ferrari and J. Robertson, "Resonant Raman spectroscopy of disordered, amorphous, and diamondlike carbon," *Physical Review B,* vol. 64, pp. 075414-075427, 2001.

[62] X. Wang, H. Q. He, D. M. Tu, C. Lei, and Q. G. Du, "Dielectric Properties and Crystalline Morphology of Low Density Polyethylene Blended with Metallocene Catalyzed Polyethylene," *IEEE Transactions on Dielectrics and Electrical Insulation,* vol. 15, pp. 319-326, 2008.

[63] L. Li, B. Li, M. A. Hood, and C. Y. Li, "Carbon nanotube induced polymer crystallization: The formation of nanohybrid shish-kebabs," *Polymer,* vol. 50, pp. 953-965, 2009.

[64] E. Piorkowska, A. Galeski, and J.-M. Haudin, "Critical assessment of overall crystallization kinetics theories and predictions," *Progress in Polymer Science,* vol. 31, pp. 549-575, 2006.

[65] M. R. Kamal and L. Feng, "Non-linear Crystalline Spherulitic Growth Behavior for LLDPE," *International Polymer Processing,* vol. 20, pp. 78-85, 2005.

[66] M. Pracella, S. De Petris, E. Butta, and M. Paci, "Polycarbonate-linear low density polyethylene blends: Thermal and dynamic-mechanical properties," *Journal of Materials Science,* vol. 25, pp. 3693-3700, August 01 1990.

[67] Z. Guang, L. Chuncheng, and L. Zhenyi, "The effects of alkali dehydroabietate on the crystallization process of polypropylene," *European polymer journal,* vol. 37, pp. 1007–1013, 2001.

[68] J. D. Hoffman, "Regime III crystallization in melt-crystallized polymers: The variable cluster model of chain folding," *Polymer,* vol. 24, pp. 3-26, 1983.

[69] M. Z. Iqbal, A. A. Abdala, and M. W. Liberatore, "Synthesis and characterization of polyethylene/oxidized polyethylene miscible blends and role of OPE as a viscosity control," *Journal of Applied Polymer Science,* vol. 133, pp. 43521-43532, 2016.

[70] Y. Gao, Y. Wang, J. Shi, H. Bai, and B. Song, "Functionalized multi-walled carbon nanotubes improve nonisothermal crystallization of poly(ethylene terephthalate)," *Polymer Testing,* vol. 27, pp. 179-188, 2008.

[71] C. C. N. de Melo, C. A. G. Beatrice, L. A. Pessan, A. D. de Oliveira, and F. M. Machado, "Analysis of nonisothermal crystallization kinetics of graphene oxide - reinforced polyamide 6 nanocomposites," *Thermochimica Acta,* vol. 667, pp. 111-121, 2018.

[72] A. Jeziorny, "Parameters characterizing the kinetics of the non-isothermal crystallization of poly (ethylene terephthalate) determined by DSC," *Polymer,* vol. 10, pp. 1142–1144, 1978.

[73] S. Liu, Y. Yu, Y. Cui, H. Zhang, and Z. Mo, "Isothermal and nonisothermal crystallization kinetics of nylon-11," *Journal of Applied Polymer Science,* vol. 70, pp. 2371-2380, 1998.

[74] C. Ferreira, C. Dal Castel, M. Oviedo, and R. Mauler, "Isothermal and non-isothermal crystallization kinetics of polypropylene/exfoliated graphite nanocomposites," *Thermochimica acta,* vol. 553, pp. 40-48, 2013.

[75] T. G. Gopakumar, J. A. Lee, M. Kontopoulou, and J. S. Parent, "Influence of clay exfoliation on the physical properties of montmorillonite/polyethylene composites," *Polymer,* vol. 43, pp. 5483-5491, 2002.

[76] S. P. Lonkar, S. Morlat-Therias, N. Caperaa, F. Leroux, J. L. Gardette, and R. P. Singh, "Preparation and nonisothermal crystallization behavior of polypropylene/layered double hydroxide nanocomposites," *Polymer,* vol. 50, pp. 1505-1515, 2009.

[77] M. Liu, Q. Zhao, Y. Wang, C. Zhang, Z. Mo, and S. Cao, "Melting behaviors, isothermal and non-isothermal crystallization kinetics of nylon 1212," *Polymer,* vol. 44, pp. 2537-2545, 2003.

[78] C. C. N. de Melo, C. A. G. Beatrice, L. A. Pessan, A. D. de Oliveira, and F. M. Machado, "Analysis of nonisothermal crystallization kinetics of graphene oxide-reinforced polyamide 6 nanocomposites," *Thermochimica acta,* vol. 667, pp. 111-121, 2018.

[79] W. Bras, I. P. Dolbnya, D. Detollenaere, R. van Tol, M. Malfois, G. N. Greaves, *et al.*, "Recent experiments on a small-angle/wide-angle X-ray scattering beam line at the ESRF," *Journal of Applied Crystallography,* vol. 36, pp. 791-794, 2003.

[80] A. Toda, R. Androsch, and C. Schick, "Insights into polymer crystallization and melting from fast scanning chip calorimetry," *Polymer,* vol. 91, pp. 239-263, 2016.

Appendix

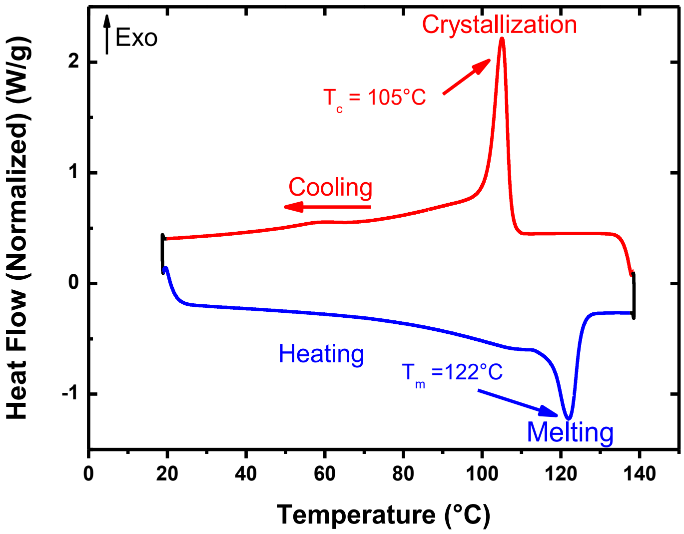

Figure 24: The cooling-heating profile for Neat PE

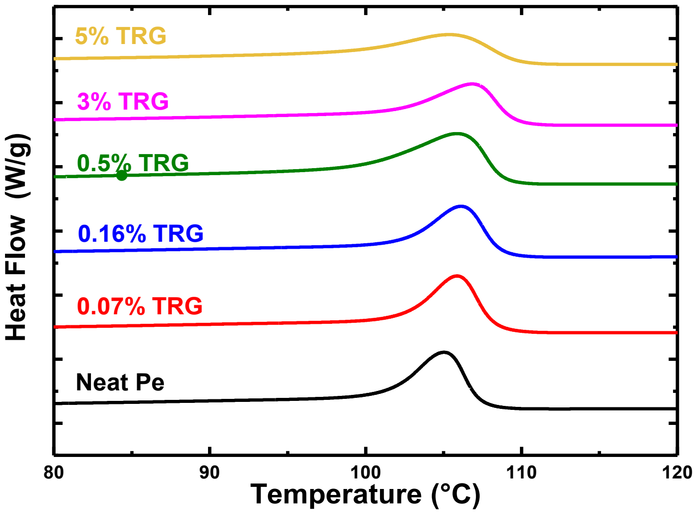

Figure 25: Heating profiles of PE/TRG nanocomposites (heating rate = 10°C/min)

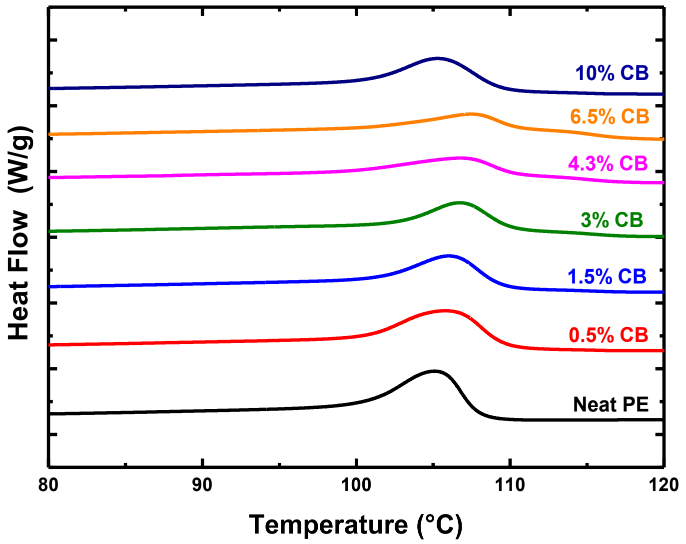

Figure 26: Cooling profiles of PE/CB nanocomposites (heating rate = 10°C/min)

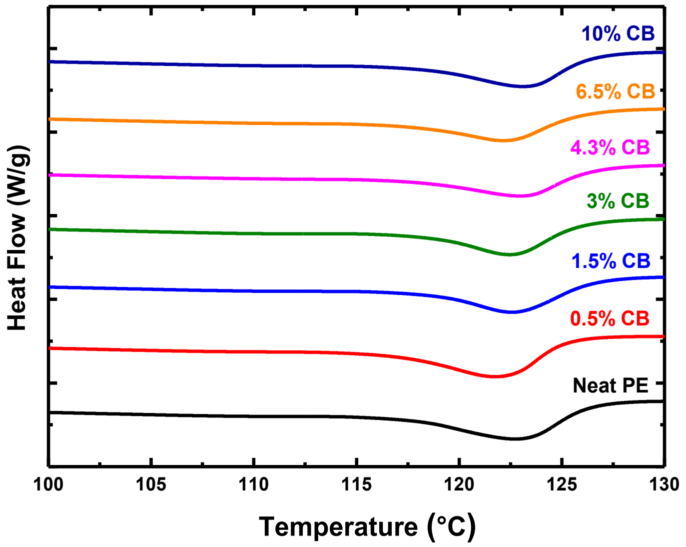

Figure 27: Heating profiles of PE/CB nanocomposites (heating rate = 10°C/min)

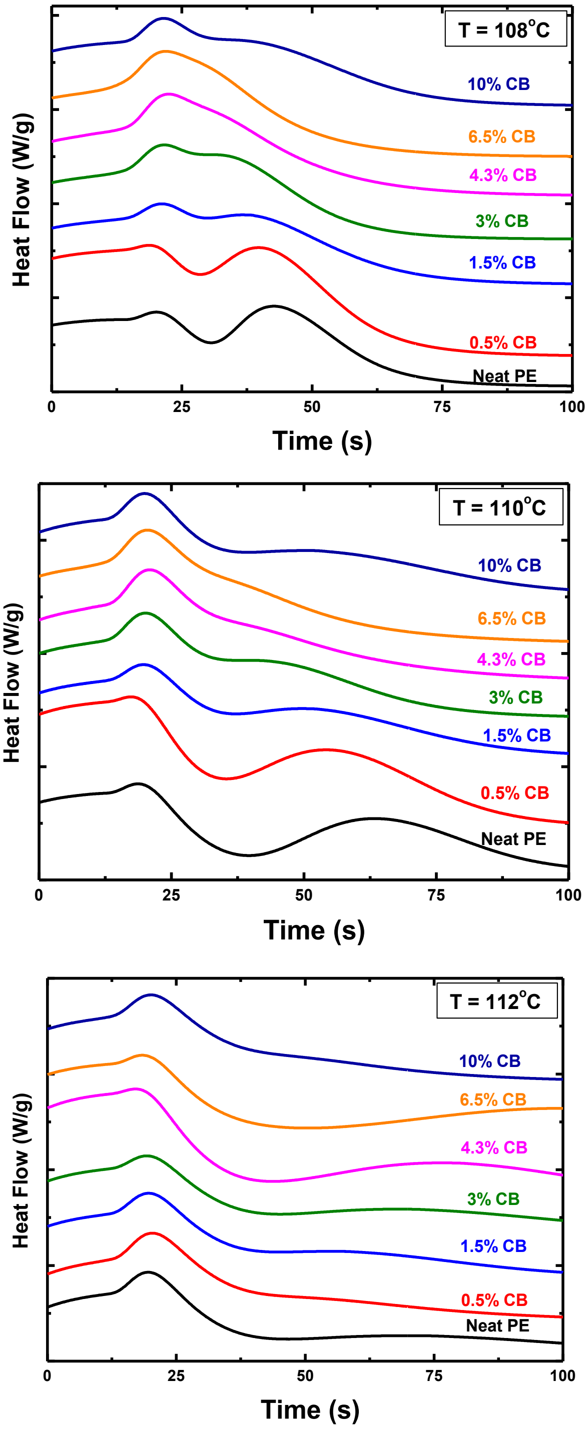

Figure 28: The isothermal experiment for PE/CB under different temperatures

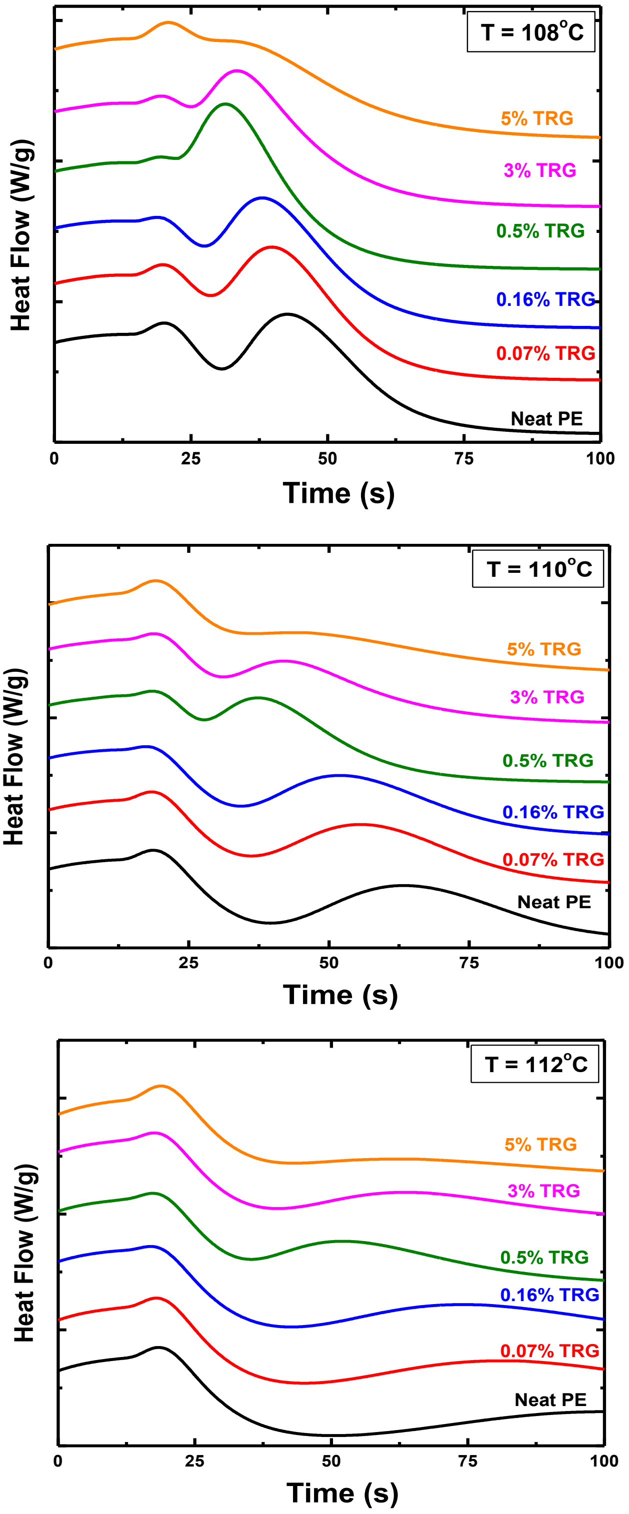

Figure 29: The isothermal experiment for PE/TRG under different temperatures

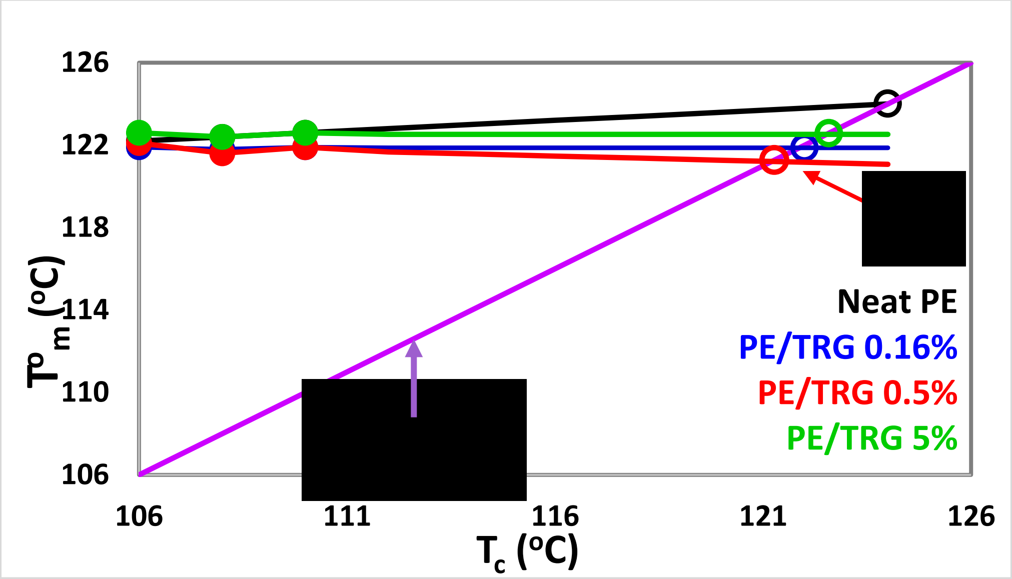

Figure 30: Hoffman-Weeks plot of PE/TRG nanocomposites

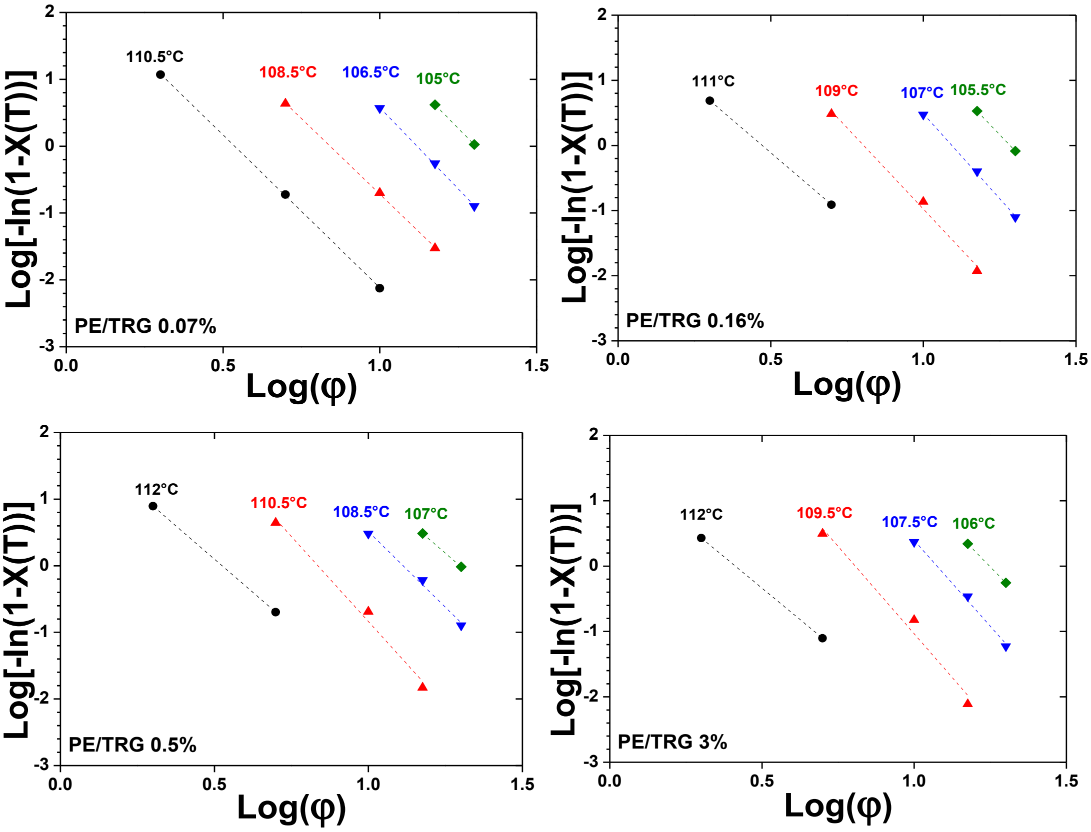

Figure 31: Ozawa plot of PE/TRG nanocomposites

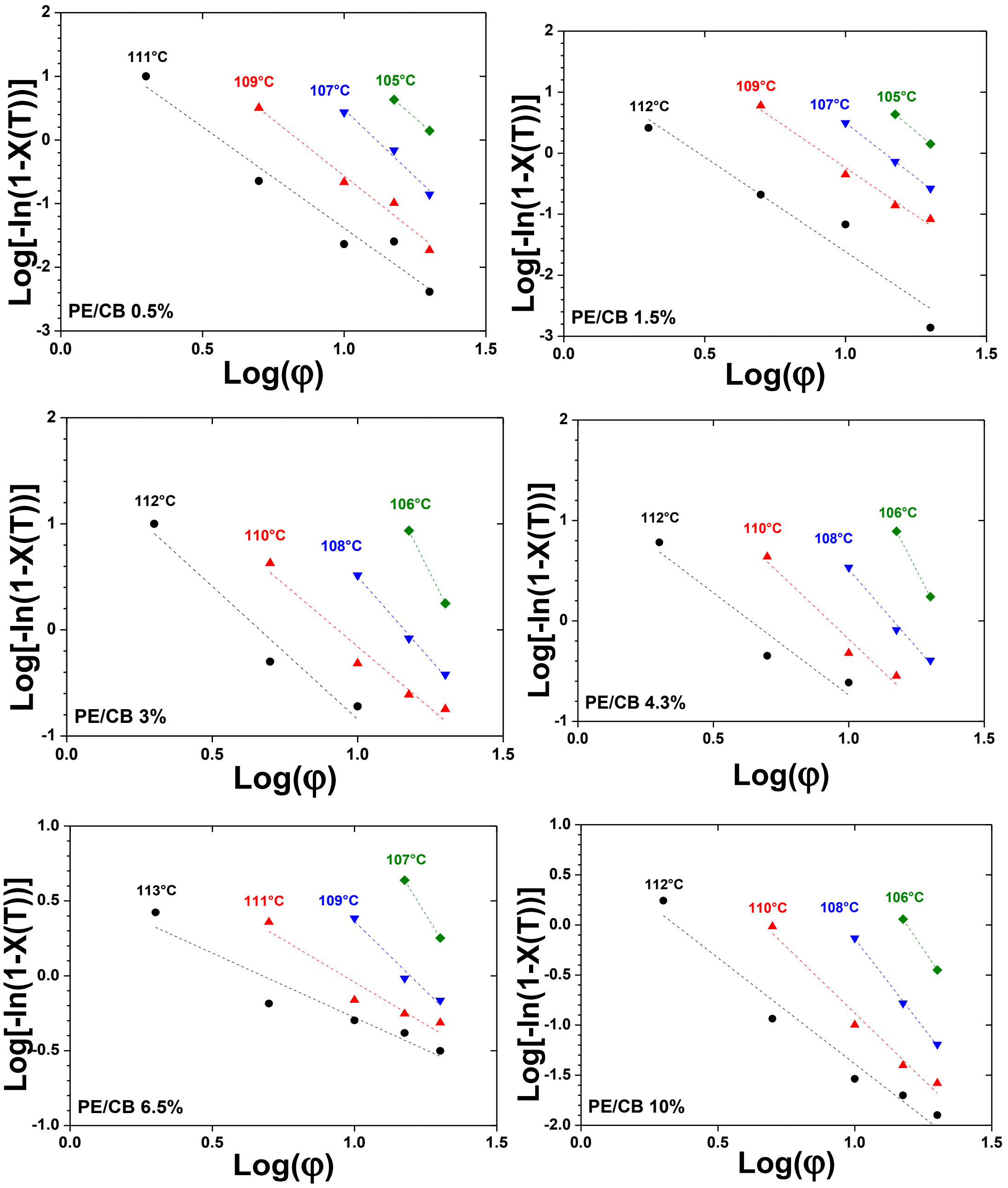

Figure 32: Ozawa plot of PE/CB nanocomposites

Table 8: The Ozawa's parameters for nonisothermal crystallization of the composites

TRG wt%	**Ozawa's constants**			**CB wt%**	**Ozawa constant**		
	T (°C)	**m**	**K (T)**		**T (°C)**	**m**	**K (T)**
0	110.5	2.3	1.6	**0.5**	111	1.2	1.8
	108	4.6	5.2		109	1.5	3.0
	106	4.1	6.7		107	2.2	4.7
	105	3.8	7.2		105	1.9	5.2
0.07	110.5	2.6	2.5	**1.5**	112	0.7	1.3
	108.5	2.5	3.8		109	1.2	2.9
	106.5	2.9	5.4		107	1.6	4.1
	105	2.8	6.2		105	1.9	5.2
0.16	111	2.0	1.9	**3**	112	-	1.3
	109	3.0	4.0		110	0.3	2.2
	107	3.2	5.7		108	1.1	3.6
	105.5	2.9	6.3		106	3.5	7.4
0.5	112	2.0	2.1	**4.3**	112	-	1.0
	110.5	3.1	4.3		110	0.1	2.0
	108.5	2.5	5.1		108	1.1	3.6
	107	2.0	5.2		106	3.2	7.0
3	112	2.9	1.6	**6.5**	113	-	0.6
	109.5	3.4	4.3		110	-	1.1
	107.5	3.3	5.7		109	-	2.2
	106	3.8	6.0		107	1.1	4.3
5	111	2.0	2.2	**10**	112	0.1	0.7
	108.5	1.7	3.3		110	0.7	1.8
	105.5	1.7	4.6		108	1.5	3.4
	104	1.3	4.4		106	2.1	4.8

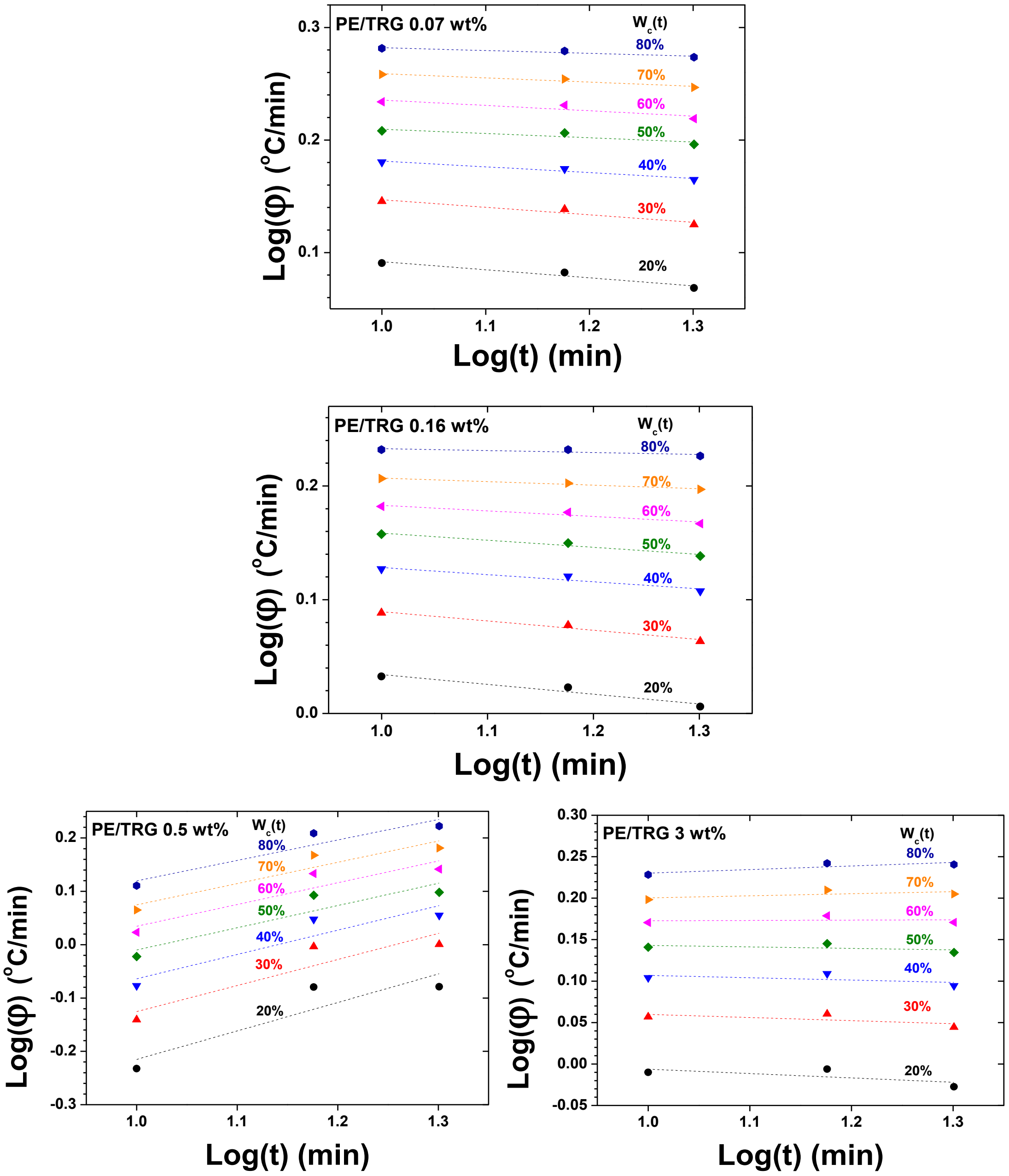

Figure 33: Liu’s plot for PE/TRG nanocomposites

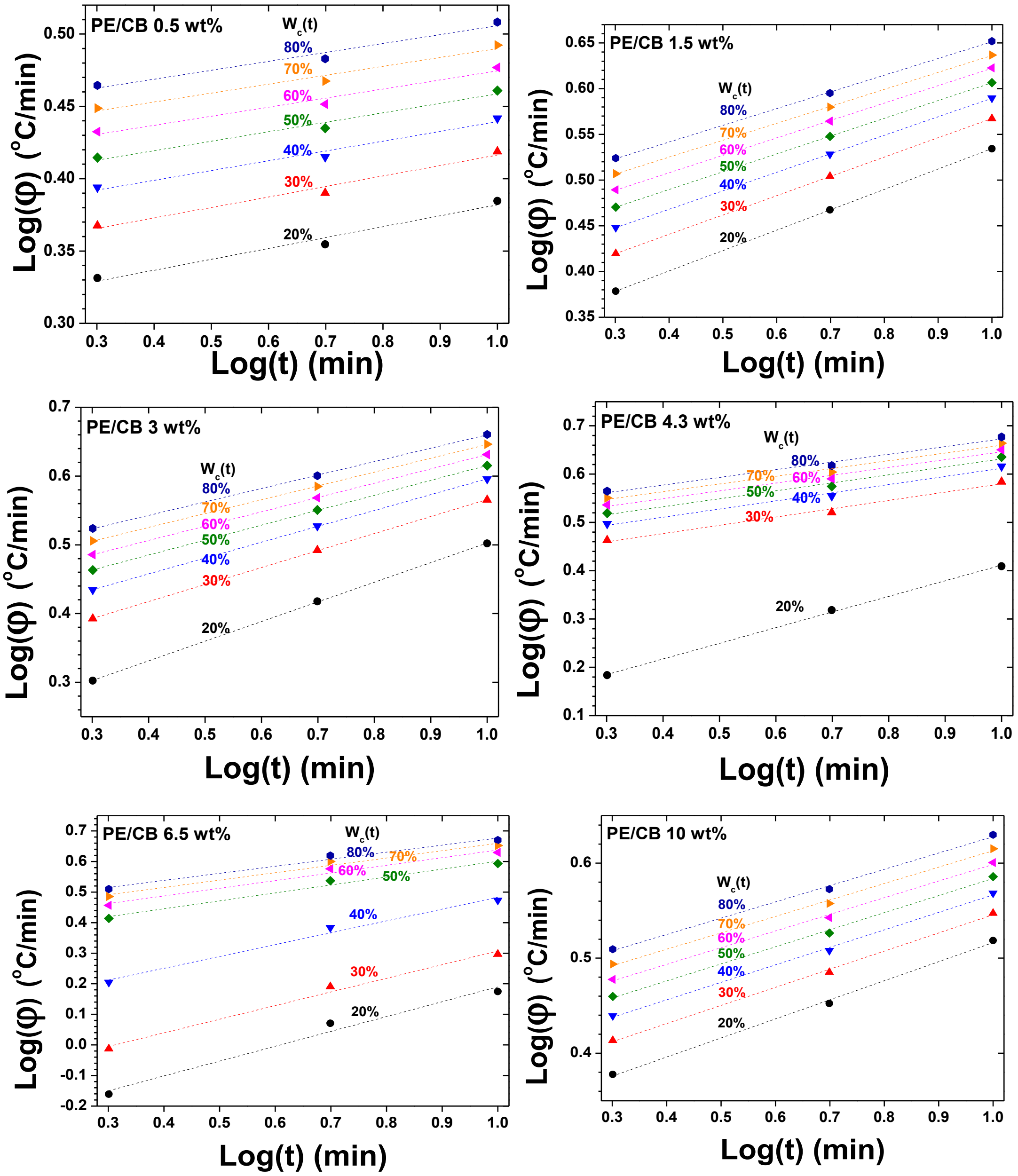

Figure 34: Liu’s plot for PE/CB nanocomposites